Defense Special Weapons Agency
Alexandria, VA 22310-3398

DNA-TR-96-12

Microelectronic Radiation Hardening Process and Design Development, Test, and Evaluation

Patrick McMarr
Akos Revesz
SFA Inc.
1401 McCormick Drive
Largo, MD 20774-5322

Reek Lawrence
Advanced Research and Applications
425 Lakeside Drive
Sunnyvale, CA 94086

March 1997

Technical Report

DTIC QUALITY INSPECTED 3

19970311 056

DESTRUCTION NOTICE:

DSWA

DISTRIBUTION LIST UPDATE

This mailer is provided to enable DSWA to maintain current distribution lists for reports. (We would appreciate your providing the requested information.)

☐ Add the individual listed to your distribution list.

☐ Delete the cited organization/individual.

☐ Change of address.

> **NOTE:**
> Please return the mailing label from the document so that any additions, changes, corrections or deletions can be made easily. For distribution cancellation or more information call DSWA/IMAS (703) 325-1036.

NAME: _____

ORGANIZATION: _____

OLD ADDRESS	CURRENT ADDRESS
_____	_____
_____	_____
_____	_____

TELEPHONE NUMBER: ( ) _____

DSWA PUBLICATION NUMBER/TITLE	CHANGES/DELETIONS/ADDITIONS, etc.)
	(Attach Sheet if more Space is Required)
_____	_____
_____	_____
_____	_____

DSWA OR OTHER GOVERNMENT CONTRACT NUMBER: _____

CERTIFICATION OF NEED-TO-KNOW BY GOVERNMENT SPONSOR (if other than DSWA):

SPONSORING ORGANIZATION: _____

CONTRACTING OFFICER OR REPRESENTATIVE: _____

SIGNATURE: _____

CUT HERE AND RETURN

DEFENSE SPECIAL WEAPONS AGENCY
ATTN: IMAS
6801 TELEGRAPH ROAD
ALEXANDRIA, VA   22310-3398

REPORT DOCUMENTATION PAGE

Public reporting burden for this collection of information is estimated to average 1 hour per response including the time for reviewing instructions, searching existing data sources, gathering and maintaining the data needed, and completing and reviewing the collection of information. Send comments regarding this burden estimate or any other aspect of this collection of information, including suggestions for reducing this burden, to Washington Headquarters Services Directorate for information Operations and Reports, 1215 Jefferson Davis Highway, Suite 1204, Arlington, VA 22202-4302, and to the Office of Management and Budget, Paperwork Reduction Project (0704-0188), Washington, DC 20503.

1. AGENCY USE ONLY (Leave blank)	2. REPORT DATE 970301	3. REPORT TYPE AND DATES COVERED Technical 910404 - 960115

4. TITLE AND SUBTITLE
Microelectronic Radiation Hardening Process and Design Development, Test, and Evaluation

6. AUTHOR(S)
Patrick McMarr and Akos Revesz (SFA); and
Reek Lawrence (ARA)

5. FUNDING NUMBERS
C - DNA 001-91-C-0054
PE - 62715H
PR - AF
TA - AK
WU - DH308950

7. PERFORMING ORGANIZATION NAME(S) AND ADDRESS(ES)
SFA Inc.   Advanced Research and Applications
1401 McCormick Drive 425 Lakeside Drive
Largo, MD 20774-5322 Sunnyvale, CA 94086

8. PERFORMING ORGANIZATION REPORT NUMBER

9. SPONSORING/MONITORING AGENCY NAME(S) AND ADDRESS(ES)
Defense Special Weapons Agency
6801 Telegraph Road
Alexandria, VA 22310-3398
ESE/Palkuti

10. SPONSORING/MONITORING AGENCY REPORT NUMBER
DNA-TR-96-12

12a. DISTRIBUTION/AVAILABILITY STATEMENT
Approved for public release; distribution is unlimited.

12b. DISTRIBUTION CODE

13. ABSTRACT (Maximum 200 words)
Radiation induced charge trapping versus Buried-Oxide (BOX) thickness on various Separation by Implantation (SIMOX) buried oxides has been determined. An inflection point has been observed in the voltage shift vs. buried oxide thickness relationship. As such, the radiation-induced voltage shifts for thin-buried-oxides are greater than what could be expected from a simple square-law relationship. These results can be explained by the location and magnitude of the radiation-induced oxide charge centroid and its relationship to the BOX thickness. The location of the centroid for trapped positive charge is dependent on the radiation-induced hole mobility, which is related to SIMOX processing as well as on geometry and charge saturation.

Photo-injection was used to study the charge trapping properties of high temperature oxidation (HITOX) SIMOX buried oxides, provided by two independent vendors. After electron injection, the electron trapping per area for both HITOX material sources was found to be larger than their respective standard (control) SIMOX structures.

14. SUBJECT TERMS
Photo-Injection
Buried-Oxide (BOX)
Oxide Charge Centroid
Electron Capture Cross Section
High Temperature Oxidation (HITOX)
Separation by Implantation of Oxygen

15. NUMBER OF PAGES
46

16. PRICE CODE

17. SECURITY CLASSIFICATION OF REPORT UNCLASSIFIED	18. SECURITY CLASSIFICATION OF THIS PAGE UNCLASSIFIED	19. SECURITY CLASSIFICATION OF ABSTRACT UNCLASSIFIED	20. LIMITATION OF ABSTRACT SAR

NSN 7540-280-5500

CLASSIFIED BY:

N/A since Unclassified.

DECLASSIFY ON:

N/A since Unclassified.

PREFACE

CONVERSION TABLE

Conversion factors for U.S. customary to metric (SI) units of measurement

To Convert From	To	Multiply
angstrom	meters (m)	1.000 000 X E-10
atmosphere (normal)	kilo pascal (kPa)	1.013 25 X E+2
bara	kilo pascal (kPa)	1.000 000 X E+2
barn	meter^2 (m^2)	1.000 000 X E-28
British Thermal unit (thermochemical)	joule (J)	1.054 350 X E+3
calorie (thermochemical)	joule (J)	4.184 000
cal (thermocemical)/cm^2	mega joule/m^2(MJ/m^2)	4.184 000 X E-2
curie	giga becquerel (GBq)*	3.700 000 X E+1
degree (angle)	radian (rad)	1.745 329 X E-2
degree Fahrenheit	degree kelvin (K)	$t_K=(t°f + 459.67)/1.8$
electron volt	joule (J)	1.602 19 X E-19
erg	joule (J)	1.000 000 X E-7
erg/second	watt (W)	1.000 000 X E-7
foot	meter (m)	3.048 000 X E-1
foot-pound-force	joule (J)	1.355 818
gallon (U.S. liquid)	meter^3 (m^3)	3.785 412 X E-3
inch	meter (m)	2.540 000 X E-2
jerk	joule (J)	1.000 000 X E+9
joule/kilogram (J/Kg) (radiation dose absorbed)	Gray (Gy)	1.000 000
kilotons	terajoules	4.183
kip (1000 lbf)	newton (N)	4.448 222 X E+3
kip/inch^2 (ksi)	kilo pascal (kPa)	6.894 757 X E+3
ktap	newton-second/m^2 (N-s/m^2)	1.000 000 X E+2
micron	meter (m)	1.000 000 X E-6
mil	meter (m)	2.540 000 X E-5
mile (international)	meter (m)	1.609 344 X E+3
ounce	kilogram (kg)	2.834 952 X E-2
pound-force (lbf avoirdupois)	newton (N)	4.448 222
pound-force inch	newton-meter (N•m)	1.129 848 X E-1
pound-force/inch	newton/meter (N/m)	1.751 268 X E+2
pound-force/foot^2	kilo pascal (kPa)	4.788 026 X E-2
pound-force/inch^2 (psi)	kilo pascal (kPa)	6.894 757
pound-mass (lbm avoirdupois)	kilogram (kg)	4.535 924 X E-1
pound-mass-foot^2 (moment of inertia)	kilogram-meter^2 (kg•m^2)	4.214 011 X E-2
pound-mass/foot^3	kilogram/meter^3 (kg/m^3)	1.601 846 X E+1
rad (radiation dose absorbed)	Gray (Gy)**	1.000 000 X E-2
roentgen	coulomb/kilogram (C/kg)	2.579 760 X E-4
shake	second (s)	1.000 000 X E-8
slug	kilogram (kg)	1.459 390 X E+1
torr (mm Hg,0°C)	kilo pascal (kPa)	1.333 22 X E-1

*The becquerel (Bq) is the SI unit of radioactivity; Bp = 1 event/s.
**The Gray (Gy) is the SI unit of absorbed radiation

TABLE OF CONTENTS

v

TABLE OF CONTENTS (Continued)

FIGURES

SECTION 1
INTRODUCTION

Various Silicon-On-Insulator (SOI), in principle SIMOX, and thermal oxide materials were evaluated for their oxide (SOI: buried-oxide) charge trapping properties over the duration of the contract. The contractual material arrived in wafer form, often only portions of a whole wafer. Quick turn-around test structures, the dual C-V and the point contact transistor (or 2ptIV), described in detail later in this report, were the benchmark vehicles for material characterization throughout this contractual effort. Two major finding are discussed below. The first has to do with the SIMOX buried-oxide charge trapping response versus buried-oxide thickness. The second observation deals with a unique post oxidation treatment to the finished SIMOX wafer, called HITOX.

Throughout this report the two findings will be discussed in parallel. The work performed in both material areas complements each other in a better understanding of the charge trapping response on the SIMOX buried-oxide.

1.1 CHARGE TRAPPING VS. BURIED-OXIDE THICKNESS.

As device geometries are scaled to smaller dimensions to the far submicron regime, the film thickness of silicon-on-insulator structures will need to be reduced. As the superficial silicon is being reduced in thickness from 300nm to 50nm, the buried-oxide thickness is being reduced from 400nm to 70nm. Will the radiation-sensitivity of the thinner SIMOX buried-oxide scale in thickness with the same relationship that holds for thermal oxides?

Thermal oxides have a known square-law thickness dependence [1], but due to large variations in material properties, the thickness dependence for SIMOX structures has remained undetermined. In earlier work, which was limited to the lower interface of standard SIMOX material (300nm<BOX<450nm), a square-law thickness dependence was observed [2]. With the availability of improved material, and new diagnostic techniques (spectroscopic ellipsometry and quick-turn-around test structures), the relationship can now be determined for the top interface and extended to BOX thicknesses below 100nm. The work in this report will cover BOX thicknesses from 68nm to 401nm.

The importance of monitoring the charge trapping response of the BOX top interface is that it is this interface that controls the back-channel transistor threshold. In fully-depleted SOI structures the front-channel transistor is electrically coupled

to the back-channel transistor. The electrical performance of SOI CMOS circuity can be severely limited by the degradation of the back-channel transistor threshold [3].

One of the purposes of this report is to enhance the knowledge of the radiation induced voltage shift of BOX material as a function of BOX thickness. This thickness relationship is needed for design and testing considerations for SOI technology as scaling in thickness occurs. The understanding of radiation induced voltage shifts as BOX thickness scales downward is important for properly designing and interpreting device measurements. Device designers need these results to aid in predicting device response, and assist in selecting approaches for radiation hardening of BOX material.

1.2 POST HIGH-TEMPERATURE OXYGEN TREATMENT OF SIMOX.

As mentioned above, additional work was performed on an unique post high temperature oxidation treatment to the finished SIMOX wafer. Several advances in SIMOX substrate fabrication are now making possible the use of the SIMOX technology for mainstream microelectronics applications [4]. This has generated an increased interest for further quality improvement of the silicon film/buried oxide. An approach taken recently is a high temperature oxidation of the finished SIMOX wafer [5,6], which was found to increase the buried oxide thickness in addition to oxidizing the top silicon film surface. Cross-sectional transmission electron microscopy (XTEM) photomicrographs indicated this high temperature oxidation (HITOX) process reduced the roughness and improved the morphology of the interface between the silicon film and the buried oxide [7].

This HITOX/BOX structure was considered to have improved material characteristics; however, the electrical properties, and in particular the charge trapping characteristics, were not evaluated. In addition to the aforementioned effort dealing with charge trapping versus BOX thickness, this report will also evaluate the electron trapping behavior of HITOX material versus standard SIMOX obtained from two separate sources. The sources will be referred to as vendor A and vendor B. It should be noted, it was not the purpose of this endeavor to compare vendor A to vendor B, but only to have two different sources of material for evaluation of a given research and development technology.

2

SECTION 2
EXPERIMENTAL

2.1 MATERIAL PREPARATION.

The SIMOX wafers arrived fully processed with respect to the SIMOX buried oxide and it's high temperature anneal. Any additional contractual processing adjustments made to the buried oxide for charge trapping modification would be classified and are not mention in this report. Below are briefly described the two main material categories, the SIMOX material and the HITOX/SIMOX material.

2.1.1 Formation of SIMOX Buried-Oxide.

The SIMOX samples used in this report were obtained from a variety of different vendors. The high-energy (120keV to 200keV) oxygen implantation dose (single and multiple) used to form the BOX ranged from 0.4×10^{18} O^+/cm^2 to 1.8×10^{18} O^+/cm^2. In all cases a post implantation anneal was performed for a standard anneal time [4].

2.1.2 The Post High-Temperature Oxygen Treatment.

In approaching the characterization of the HITOX technology, a SIMOX control was selected for comparison. The samples were processed in a similar fashion as those in previous publications [2,4]. The SIMOX wafers were formed by a standard process [5,7]. The resulting thicknesses of the buried oxides were 97.5nm for vendor A, and 103nm for vendor B. This thickness range is considered thin for SOI material and is currently gaining importance [8]. Following the formation and anneal of the BOX (the finished SIMOX wafer), the HITOX process is performed. From spectroscopic ellipsometry measurements, it was found [9] that the HITOX process increased the BOX thickness by 25nm for vendor A and 5nm for vendor B.

2.2 DEVICE FABRICATION.

The material evaluated throughout this report arrived in whole or portion of wafer form. The SIMOX wafers were finished SIMOX wafers (BOX formed, and high-temperature anneal performed). Using our simple processing procedures, quick turn around test structures were fabricated. Listed below are three of the principle test structures fabricated for material evaluation.

2.2.1 Dual C-V Structure.

The dual capacitance-voltage C-V device was a fundamental structure used throughout this work. The first device fabrication step was to deposit aluminum dots onto the SIMOX top silicon film. These aluminum gates were than used as a mask for

3

a hydrazine etch which removed the surrounding top silicon film
down to the buried oxide. The finished structure was an aluminum
gate on top of a silicon island, which resided on top of the
buried oxide and silicon substrate. Figure 2-1 a) shows the
Al/Si/SiO$_2$/Si structure, or the dual C-V device.

2.2.2 Point-Contact Transistor.

The point contact transistor (or 2ptIV, for two point current
voltage) was also a fundamental structure used throughout this
work. The fabrication of the point contact transistor was
similar to the above dual C-V structure. First the SIMOX wafer
had aluminum dots deposited on the top silicon film. These
aluminum gates were than used as a mask for a hydrazine etch
which removed the surrounding top silicon film down to the buried
oxide. (At this point, the structure is identical to the above
capacitance C-V dot.) Next, the aluminum gate was removed. The
remaining structure was an isolated silicon island. The height
of the silicon island depended on the arriving top silicon film

a) Dual C-V   b) Point-contact transistor
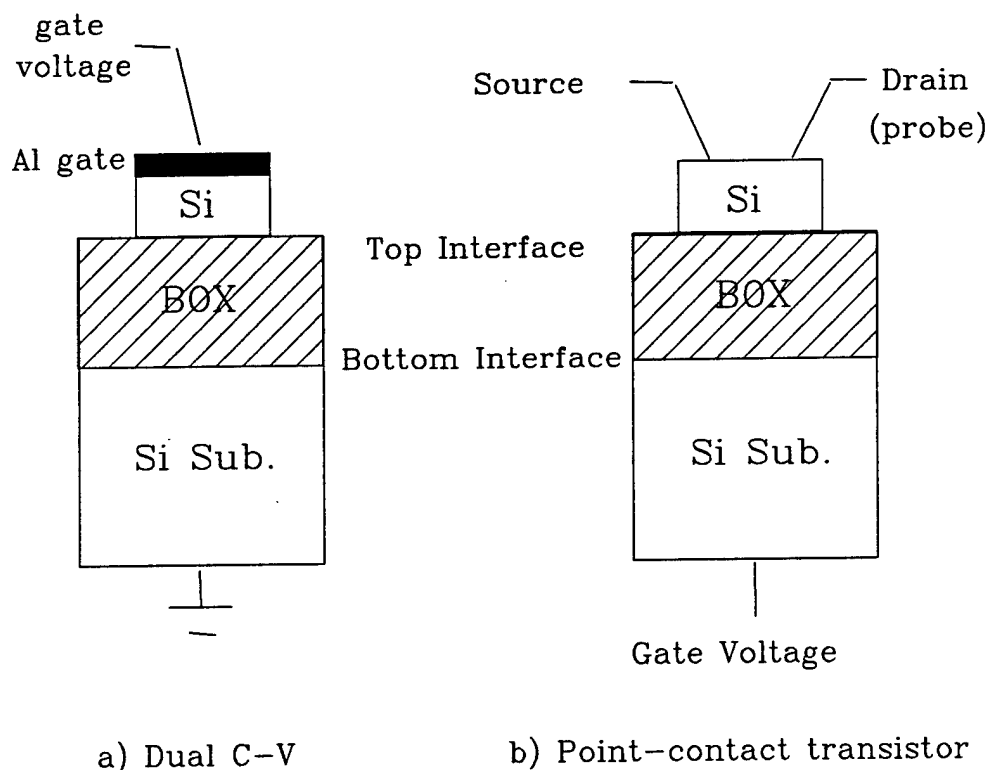
Figure 2-1. Simple diagram of the SIMOX a) dual C-V structure,
and b) the point-contact transistor.

4

thickness. This isolated silicon island was the finished
structure. Two probes were placed upon the top silicon
(approximately 5mil apart) acting as source and drain, and the
wafer substrate acted as the gate. With the buried oxide acting
as the gate oxide, the device response was that of a MOSFET
transistor from weak-midgap to strong inversion for both carrier
types. Figure 2-1 b) shows the finished point contact
transistor.

2.2.3 Photo I-V Structure.

Fabrication of the photo I-V structure requires the removal of
the top silicon film [10,11]. With the BOX exposed, large but
thin aluminum gates were deposited. The aluminum gate allows the
structure to perform as a capacitor (the largest of the gate is
need for measurable electron injection current levels), and the
thin aluminum gate allows the 5ev mercury light to pass through.
The finished photo I-V structure is shown in Figure 2-2.
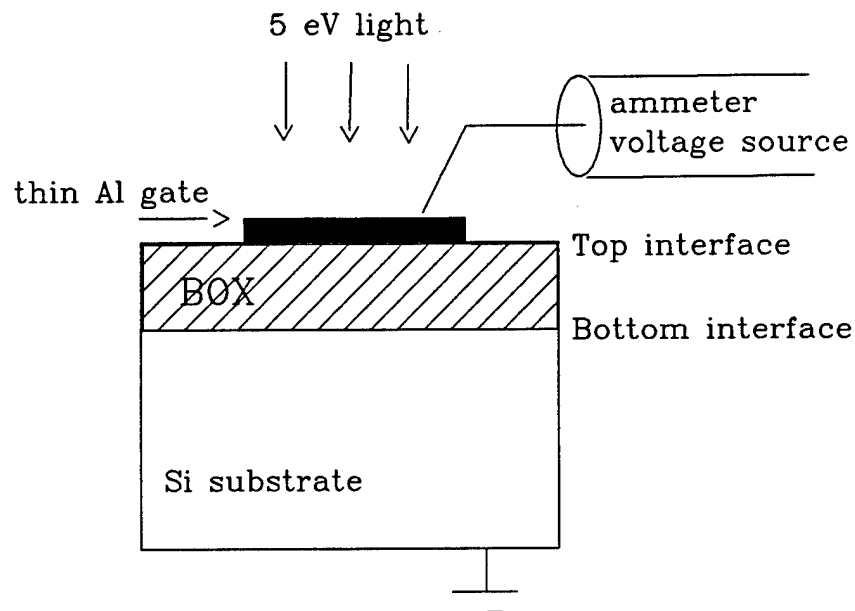
Figure 2-2. The SIMOX photo I-V structure used for photo-
injection.

2.3 EQUIPMENT.

The equipment used throughout this effort was all part of an advanced computer controlled semiconductor parameter analysis system. Each measurement capability was automated by computer code for controlled data collection. Listed below are descriptions of select sub-systems that were used to characterize delivered material throughout the reported period.

2.3.1 Capacitance and Current Measurement Equipment.

The computer automated data acquisition of capacitance and current versus voltage data routines were controlled by a Hewlett Packard (HP) model 9000 series 300 computer. The capacitance vs voltage data was collected by any of the following; a HP 4280A 1Mhz C meter, HP 4274A or HP 4275A multi-frequency LCR meter. The current vs voltage data was collected by any of the following; a Keithley 617 ammeter, a HP 4140B pico-ammeter, or a HP 4145A semiconductor parameter analyzer.

2.3.2 X-Ray Source.

To generate electron/hole pairs in the buried oxide, thus creating oxide trapped charge, our samples were exposed to 10 KeV

X-rays from an ARACOR 4100 X-ray source. The dose rate was variable, but the standard dose rate was $1800rad(SiO_2)/sec$. The samples were exposed in a total dose fashion to total doses as high as $10Mrad(SiO_2)$. The standard dose was $1Mrad(SiO_2)$. All sample biasing, irradiations, and measurements were done by probecards at room temperature.

2.3.3 Photo-Injection Equipment.

The photo-injection system is more complex than the other mentioned data acquisition systems. The light source, which yields the needed energy for electron injection, must be shutter controlled. With the lamp on and shutter open the electron injection current must be monitored, then intermittently the shutter must be closed to allow for capacitance monitoring. The controlling computer is the above mentioned HP system. The capacitance and current meters are also the same as mentioned above. The light source was an Oriel 500 watt mercury lamp powered by a Oriel 68810 arc lamp power supply.

2.4 METHODS OF INVESTIGATION.

A variety of techniques were used to characterize the charge trapping of the buried oxide. Listed below are three principle techniques used. Each section briefly describes a technique, and the expected results obtained by using the technique.

2.4.1 Capacitance-Voltage Method.

The capacitance versus voltage technique is a standard for monitoring trapped charge in the oxide [12]. Since the SIMOX buried oxide is known the exhibit bulk oxide trapping [13], the dual C-V structure is ideal for top and bottom voltage shift parameter extraction. The ratio of the voltage shifts also yields a charge centroid [12].

The SIMOX wafer lends itself naturally for the dual C-V structure. The problems arise in data extraction though. Often the top interface is difficult to identify, due to doping differences between top silicon film and bottom silicon substrate. The bulk of the work presented here is done n-type top silicon and p-type silicon substrates. The bottom C-V curve is clear and data extraction is excellent. The top C-V curve is often a bit more evasive, but with good correlation between the top C-V shift and that of the point-contact transistor confidence in the top C-V shift is obtained. In general, only a ΔV_{mg} is monitored for the top and bottom interface. Additional information is not necessary for material characterization at these stages of investigation.

2.4.2 Current-Voltage Method.

The principle technique used to characterize the material provided was the two-point-current-voltage (2ptIV) technique (sometimes referred to as: point contract or quick-turn-around structure (QTA)). When introduced, this new measurement technique demonstrated a fast turn-around testing capability for the top interface of SIMOX material [14,15]. Later the current-voltage data was shown to be consistent to that of a finished transistor [16]. The 2ptIV technique was used throughout this effort, and the test structure is shown in Figure 2-1 b).

Typical 2ptIV and dual C-V (n-type top Si, and p-type bottom Si) characteristics before and after radiation are shown in Figure 2-3. The BOX structure used in Figure 2-3 is a typical medium BOX thickness structure (T_{BOX}=164nm). Note that both the 2ptIV and the dual C-V structure yield the same top interface voltage shift information. This is a key correlation to support the use of the 2ptIV technique throughout the effort.

Additional validity of the 2ptIV technique can be shown by comparing C-V and 2ptIV charge trapping results for the a variety of samples. Figure 2-4, shows this comparison for ground bias as well as for biased data. The two techniques yield the same voltage shift information. Thus, for charge trapping information on the top interface, the 2ptIV technique has been used in this effort for material evaluation.
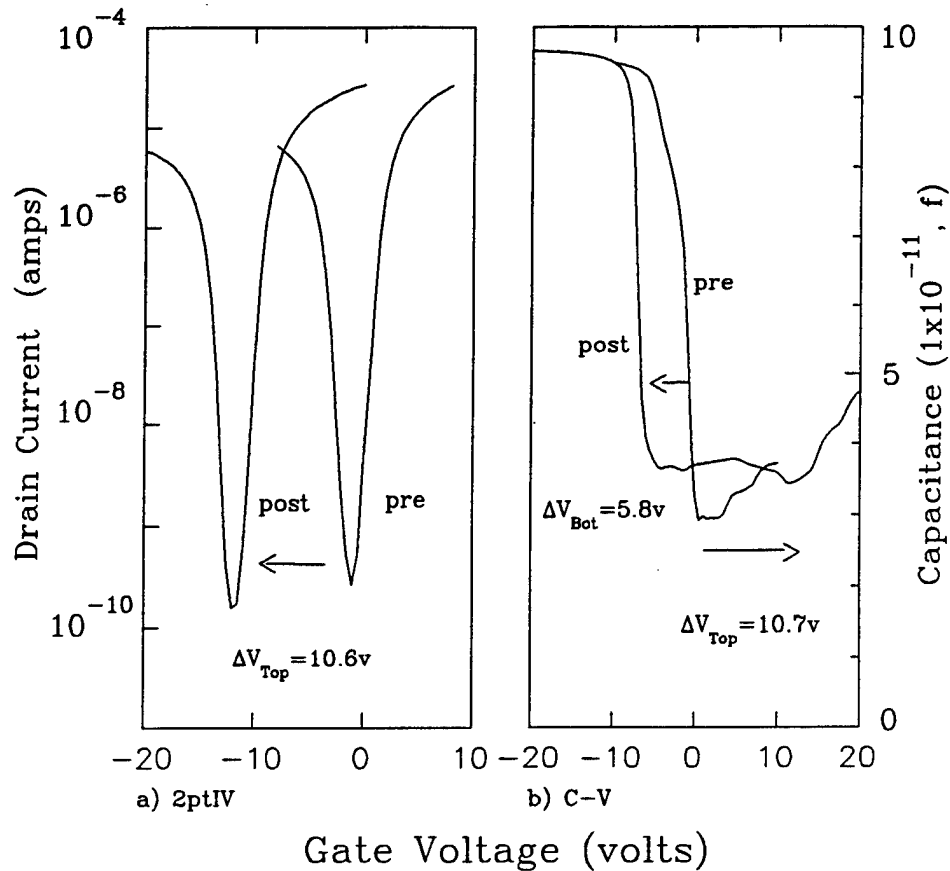
Figure 2-3. Sample results after 1Mrad (SiO2) with V_{BG}:+5×10⁴
V/cm, a) 2ptIV results, and b) dual C-V results.

2.4.3 Photo-Injection Method.

Electron trapping in the BOX was investigated with the use of the
photo injection technique. The photo-injection structures, as
mentioned earlier, were fabricated by removing the top silicon
layer, and depositing a thin (20nm) aluminum gate. The structure
represents a capacitor with a thin gate, the thinness of the gate
allows the mercury light to pass through. A Oriel 500 watt
mercury lamp supplies the energy for electron injection into the
oxide, and is filtered to prevent hole injection (Oriel filter
59418). For the work presented in this report, a constant
electron injection current density of $1×10^{-7}$ A/cm^2 was maintained
for approximately 42 hrs by varying the negative applied gate
voltage, causing electron injection from the aluminum gate. The
applied field remained under 0.5 MV/cm.

The electron trapping behavior within the BOX was evaluated by
capacitance and photo-current measurement techniques. The midgap

8
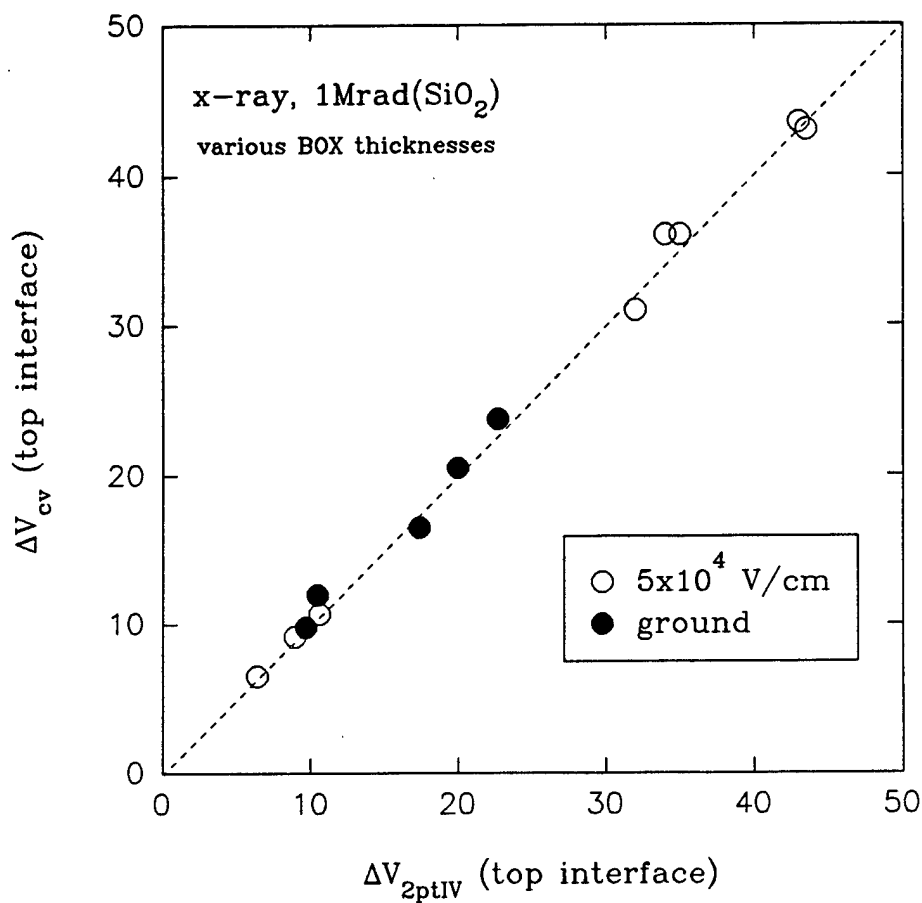
Figure 2-4. A comparison of top interface voltage shifts for the C-V and the 2ptIV techniques.

capacitance of the capacitor is monitored as a function of electron injection (a ΔV_{mg} vs injection-time is recorded). From this data an electron capture cross section can be determined [7]. Finally, from the photo-injection I-V curve, the total number of occupied electron trap and a charge centroid can be determined [12].

SECTION 3
EXPERIMENTAL RESULTS

3.1 CHARGE TRAPPING IN BURIED-OXIDES.

For SOI circuits in space bound systems, fringing fields in the BOX are of extreme importance for BOX charge control. Charge buildup within the BOX effects the threshold voltage of the back-channel transistor. The pass-gate bias condition, where both the source and drain are in the "high" bias condition (V_{dd}=high (+5v)) is considered the worst case bias condition for total dose testing. It is the fringing fields due to this bias condition that wrap-around and are terminated at the back-channel interface that cause the greatest device degradation. These fringing fields cause radiation-induced positive charge to drift to the back-channel interface, where it is then trapped. Here the positive trapped charge lowers the back-channel threshold of N-channel transistors, which in turn affects the front-gate-channel FET operation. Controlling, as well as predicting, the charge trapping behavior of the BOX is of extreme importance to ensure proper operation in a radiation environment.

Modeling work by Smith found that the SOI fringing field in the BOX oxide for V_{dd} "high" was an electric field of 5×10^4 V/cm [6]. Our BOX testing has focused on this fringing field effect within the BOX. The test structures have been evaluated with a substrate bias of 5×10^4 V/cm to simulate the fringing field BOX effect.

3.1.1 Charge Trapping vs. Electric Field.

The polarity and magnitude of the applied electric field across an oxide under the influence of ionizing irradiation will effect the charge trapping results [17,18]. For our dataset of SIMOX wafers the effects are of importance since the buried oxide differs so from that of a thermal oxide [19]. The effect of electric field on BOX charge trapping for a sample in our SIMOX dataset is shown in Figure 3-1. The ΔV_T voltage shifts are from point contact transistor results (the top interface) on a thick BOX structure (T_{BOX}=400.9nm). The influence of the applied electric field during irradiation on BOX charge trapping begins at 1×10^4 V/cm and is very strong by 1×10^5 V/cm. These fields are in reference to the substrate (positive bias to substrate). The work presented throughout this report on voltage shifts versus BOX thickness will cover biases from -5×10^5 V/cm to 5×10^5 V/cm. Again, the emphasis of this effort was V_{BG}:$+5\times10^4$ V/cm, simulating typical device application BOX electric fields.

10
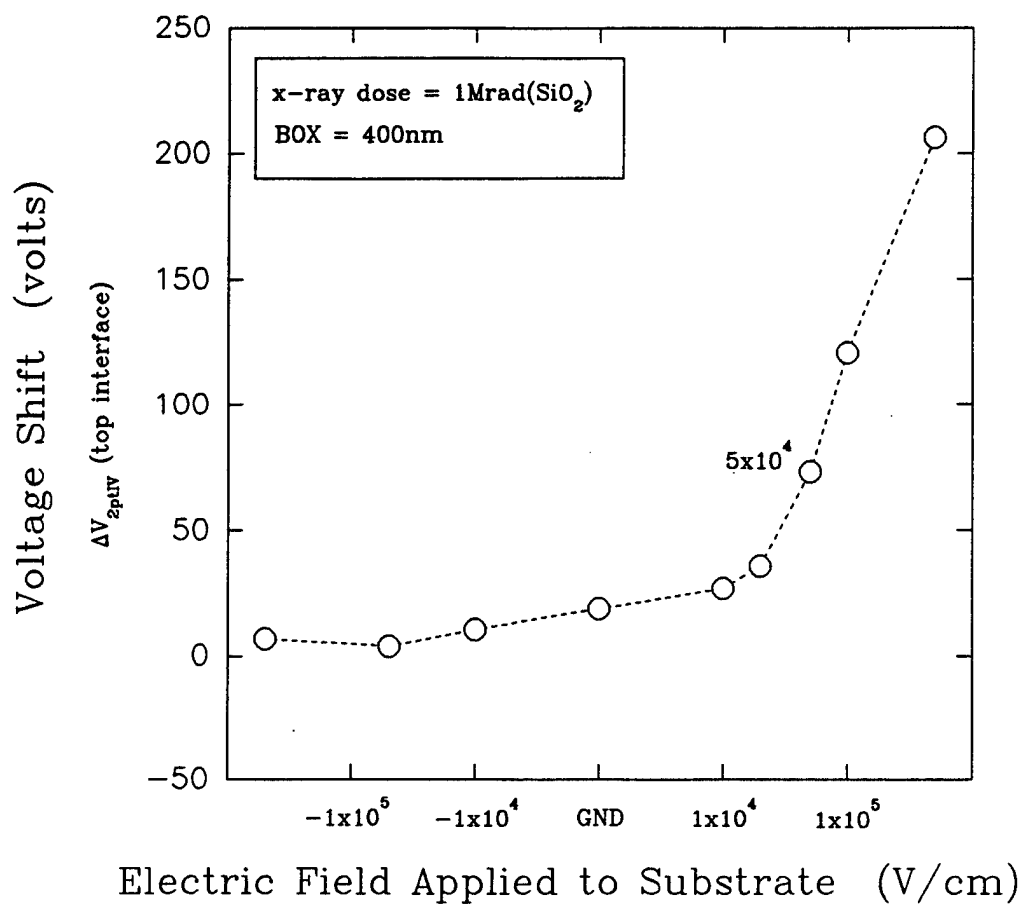
Figure 3-1. Voltage shift versus applied electric field for a dose of 1Mrad (SiO$_2$).

3.1.2 Charge Trapping vs. Buried-Oxide Thickness.

In efforts to compare a variety of SIMOX buried oxide technologies we have gathered a large database of BOX charge trapping results for V_{BG}: $+5 \times 10^4$ V/cm at 1Mrad(SiO_2).

Figure 3-2 shows a plot of point-contact (top interface) voltage shifts for various BOX thicknesses. The entire dataset is shown in Figure 3-2.
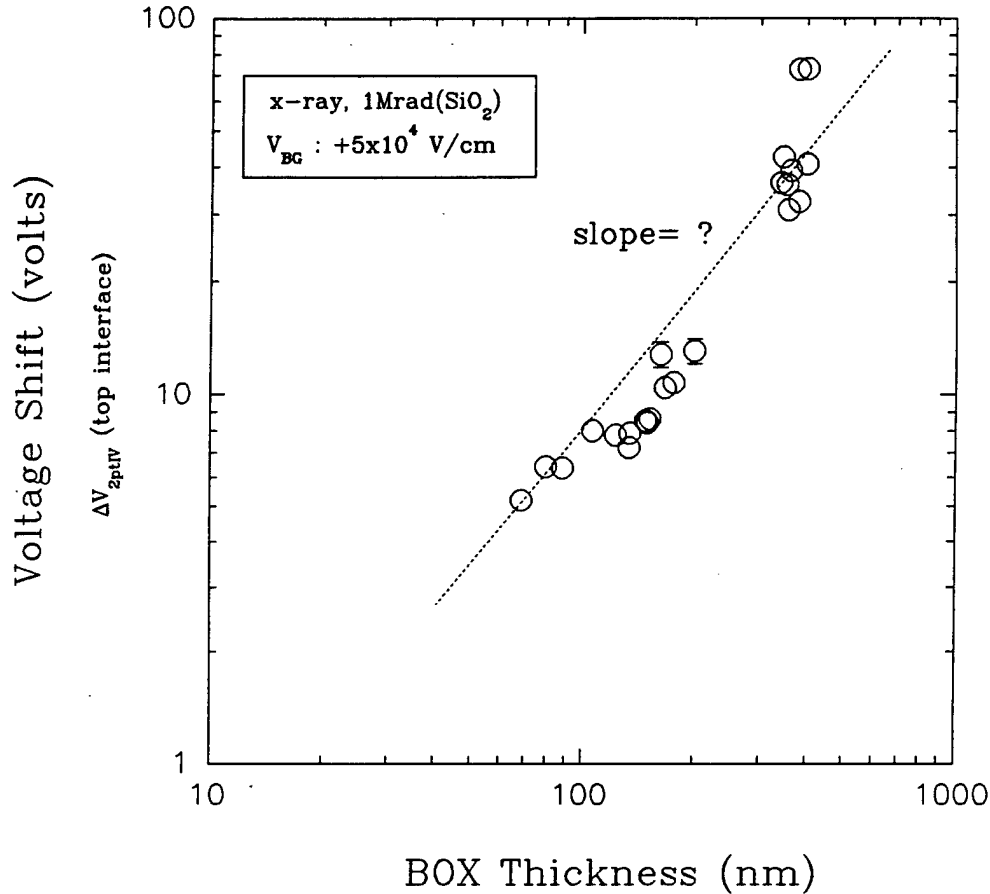
Figure 3-2. Voltage shift versus BOX thickness for VBG:$+5 \times 10^4$ V/cm at 1Mrad (SiO_2), (all data included).

A primary research goal would be to extract a relationship from Figure 3-2, (graphical at the minimum) that would allow the prediction of the radiation response of SIMOX structures. A

first attempt would be to represented the dataset by a line with unity slope, (as shown in Figure 3-2). Although, scatter in the data causes some uncertainty, and knowing that SIMOX radiation results vary greatly with processing, the graph basically raises more questions than it answers. Later in this report these questions and research approaches will be addressed.

3.1.3 Charge Trapping vs. Density of Buried-Oxide.

For help in interpreting Figure 3-2, we revisited the work published by Mrstik [20]. This work compared radiation charge trapping for SIMOX BOX oxides versus an optically determined BOX density (spectroscopic ellipsometry (SE). The results were found
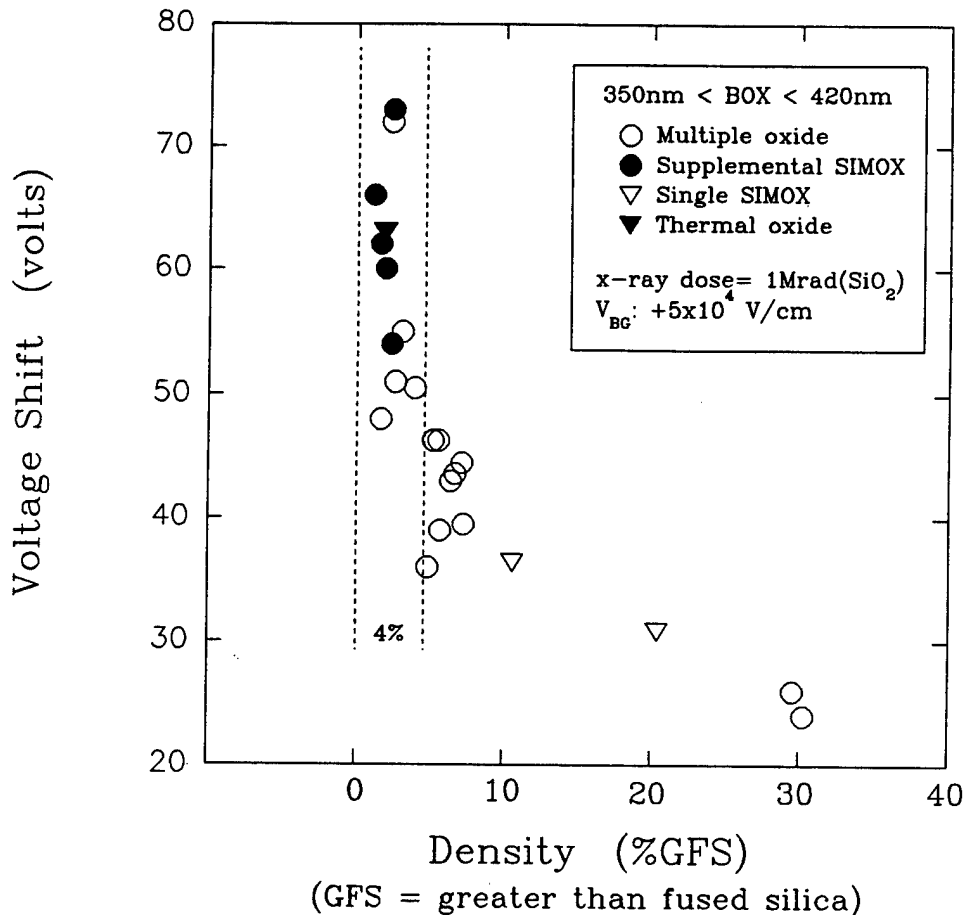
Figure 3-3. Voltage shift versus BOX density for thermal oxide and various SIMOX structures (reprint from: B.J. Mrstik [20]).

useful in analyzing our dataset. For clarity, Figure 3-3 is an annotated graph from the Mrstik publication showing the strong charge trapping variation versus a BOX density parameter.

All the samples evaluated throughout this report were characterized by the spectroscopic ellipsometry technique [9]. The optically determined density did vary among our sample dataset and material suppliers. The SE technique was also considered very accurate in determining the BOX thickness. It should be noted, this contractual effort relied largely on transistor ΔV_T BOX shifts for evaluating the charge trapping response of the buried oxide (which is fine, and necessary), but the value of the SE results should be underscored.

3.2 ELECTRON TRAPPING IN BURIED OXIDES.

The use of ionizing irradiation (X-rays) to generate electron/hole pairs within the SIMOX buried oxide usually results in a net trapped positive charge. To investigate the influence of only electron trapping on the charge trapping behavior of the BOX, the technique of photo-injection was implemented. Here only electrons are injected into and trapped within the oxide. The BOX can now be evaluated as to solely electron trapping behavior. The results below compare the electron trapping results of a standard SIMOX to a recent post-oxygen treatment applied to SIMOX.

As mentioned earlier, during the photo-injection process the midgap capacitance is monitored to evaluate the electron trapping of the BOX. With the 5ev mercury light on, and using a computer to continually adjusting the applied gate voltage to maintain a constant injection current level, the electron injection process proceeds. The computer records a capacitance ΔV_{mg} as a function of injection time (or fluence). Note, this capacitance information is from the lower (bottom) interface, and the motion of this ΔV_{mg} will saturate in time. The magnitude and shape of this ΔV_{mg} vs fluence curve is the key information extracted for the photo-injection technique.

Figure 3-4 shows the photo-injection results for both HITOX material sources with their respective control SIMOX structures. The y-axis, the midgap (ΔV_{mg}) voltage shift, has been converted into a -charge/area (electron trapping) to normalize out any thickness dependencies, and the x-axis, time of electron injection, has been converted into a number of injected electrons per area (N_{inj} cm^{-2}, a fluence). Both vendors' HITOX structures show more electron trapping per area than their respective control SIMOX structure, indicating that the HITOX process increases the electron trapping response for both vendors baseline technology. Figure 3-5 (a,b) shows the pre and post C-V curves, post referring to the end of the entire electron injection sequence. The post C-V curves show no stretch-out, and

14

therefore interface states, or lateral non-uniformity effects, can not account for the HITOX increase in electron trapping.
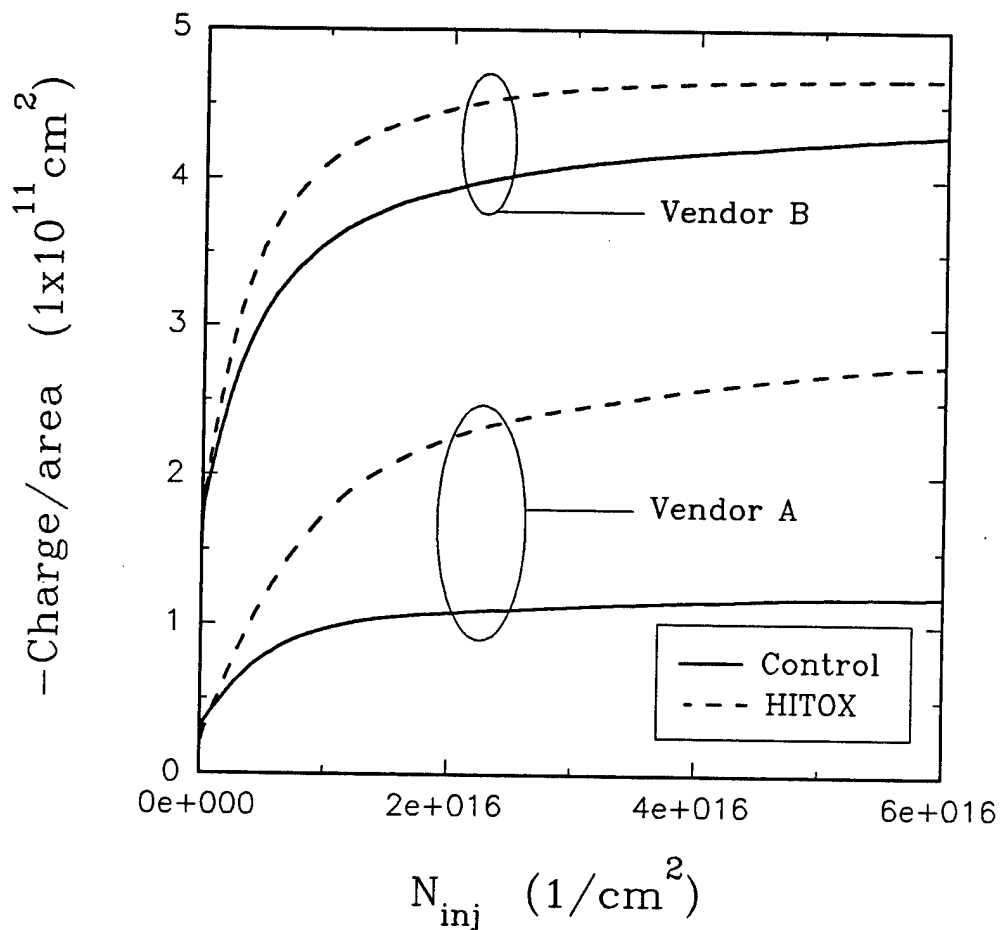

Figure 3-4. The photo-injection results for standard SIMOX and HITOX for two separate vendors. The HITOX indicates more electron trapping than the standard SIMOX material.
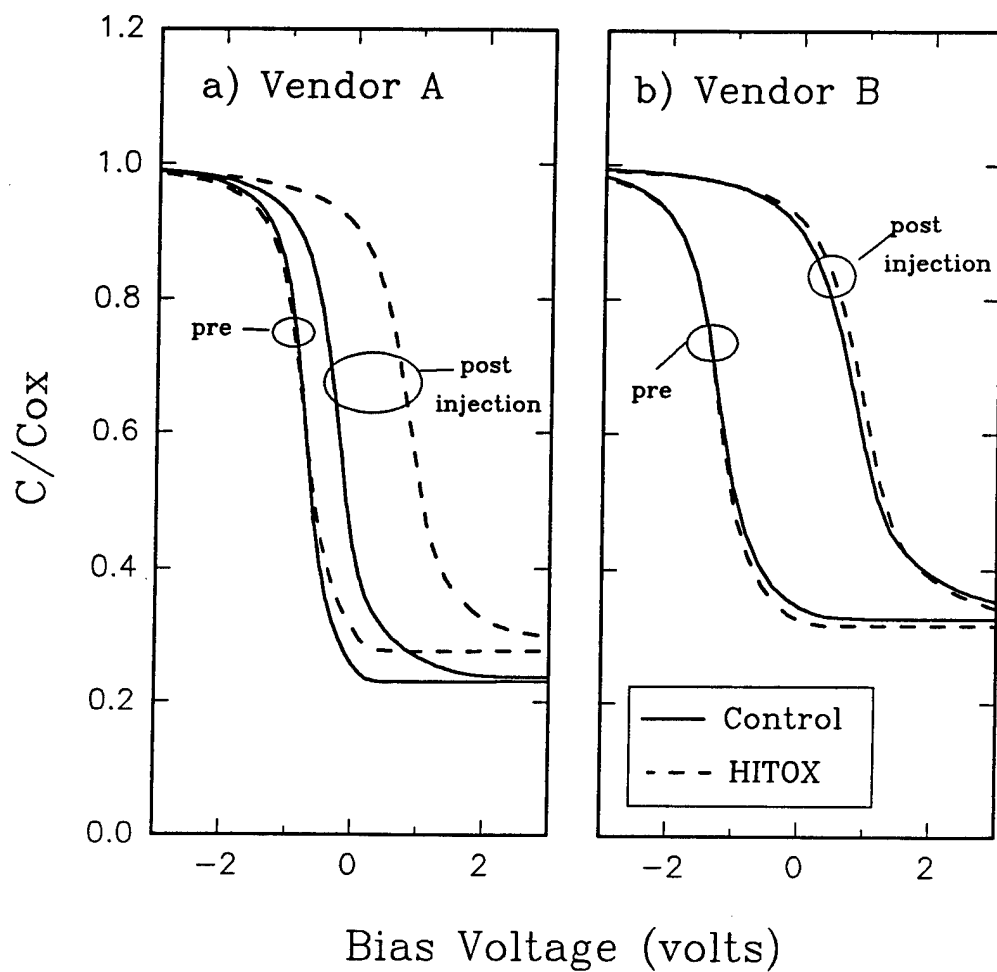
Figure 3-5. The capacitance-voltage curves for pre- and post-electron injection for standard SIMOX and HITOX for a) vendor A, and b) for vendor B.

SECTION 4
DISCUSSION AND ANALYSIS

4.1 LACK OF SQUARE-DEPENDENCE IN THICKNESS RELATIONSHIP.

By considering the results of the Mrstik et al. work on charge trapping vs. density of the BOX on similar SIMOX material, our dataset in Figure 3-2 has been re-evaluated. We selected only those samples from our dataset which had a density close to that of a thermal oxide. The assumption being that BOX with densities close to thermal oxide would behave like thermal oxide. This was supported by the wide variation in radiation induced voltage shifts observed for similar thickness samples but varying in BOX density. For instance, at a given BOX thickness, such as 430nm, the radiation induced shift was observed to vary, depending on BOX density, from 40 to 85 volts. Using the spectroscopic ellipsometry (SE) technique, we selected only those samples which had a low density (near to a thermal oxide, less than 4% Greater than Fused Silica (GFS), (density<4%GFS).

By selecting a narrow range of densities (density<4%GFS) our dataset from Figure 3-2 has been re-evaluated. Figure 4-1 shows the voltage shift versus BOX thickness for these samples with near thermal oxide density. Note the inflection point in Figure 4-1, which begins at about 180nm (the inflection point refers to the region of data with slope=0.7, the non-square-law portion). When an oxide is exposed to ionizing irradiation, there are known processes that take place; namely, the motion of radiation induced electron/hole pairs under the influence of an applied electric field, and secondly recombination within the oxide. The two processes are in competition with each other. It is known that in high density SIMOX the radiation induced holes are not mobile [20,21], in low density SIMOX the holes are mobile [20,13,22]. The value of mobility of the radiation induced holes in low density SIMOX is unknown, and beyond the scope of this work. Nevertheless, the mobility of these holes play an important role in the observed electrical voltage shift at the top interface of the BOX. More will be mentioned later on the role and influence of these radiation induced holes on the observed inflection point.

4.1.1 Location of Charge Centroid.

To better understand the observed inflection point for the V_{BG}:+5×10^4 V/cm data, a few selected dual C-V structures were also irradiated (a thin=80nm, medium=164nm, and thick=350nm). The dual C-V structure yields voltage shift information for both top and bottom BOX interfaces. From these dual C-V structures a charge centroid was extracted, using the following equation [12,23]:

$$\chi = T_{BOX} * (1-\Delta V_{top}/\Delta V_{bot})^{-1} .$$

17
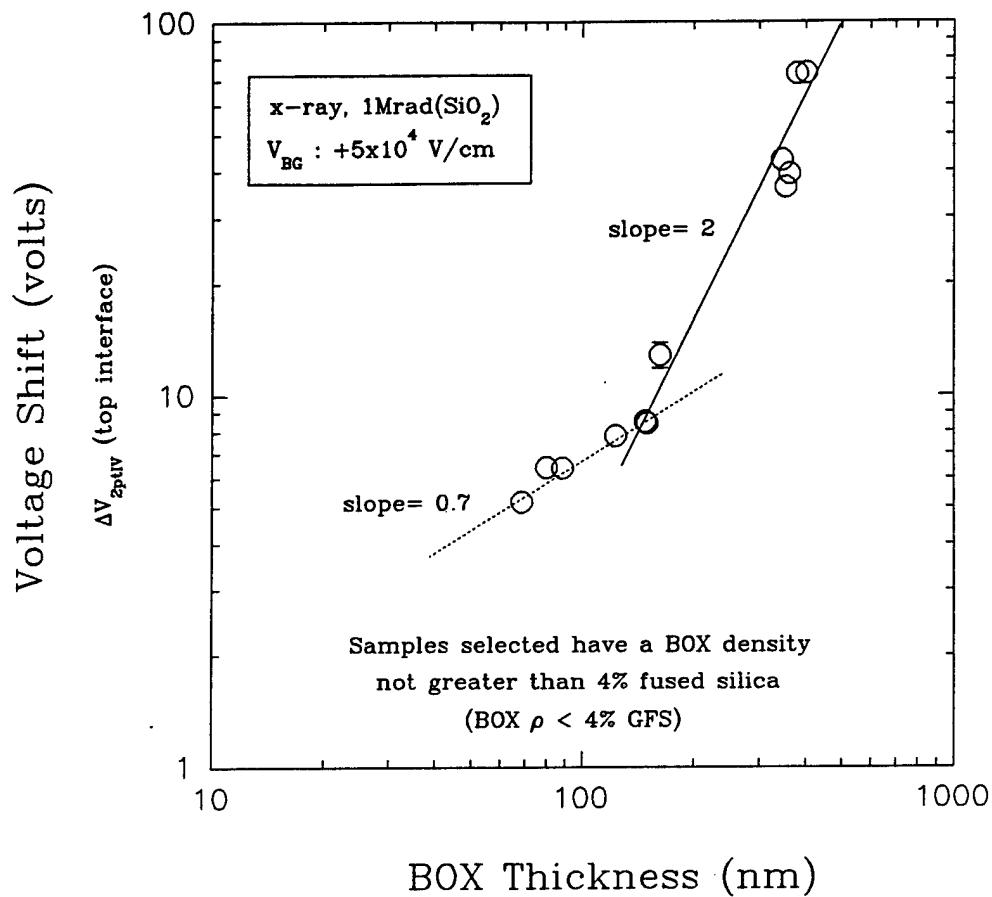
Figure 4-1. Replot of Figure 3-2 with using a density limitation.

Figure 4-2 shows the centroid data in a bar chart format. The key observation from the centroid measurements is that the centroid location has a thickness dependence. All three thicknesses appear to trap the same level of charge, 4×10^{-7} C/cm^2, at 1Mrad(SiO$_2$). The key difference is the location of the centroid. Namely, the thin BOX sample has its centroid at 34nm; whereas, the thick has its centroid at 76nm. The location of the BOX centroid vs. thickness must be a material property, since we still observe a similar phenomena at saturation (shown later in this report). The observation that all three thicknesses have approximately the same trapped oxide charge is probably related to hole mobility and trap concentration limitations. Since the holes in the thick BOX relative to the thin BOX have to move farther to reach their centroid location (almost a factor of six
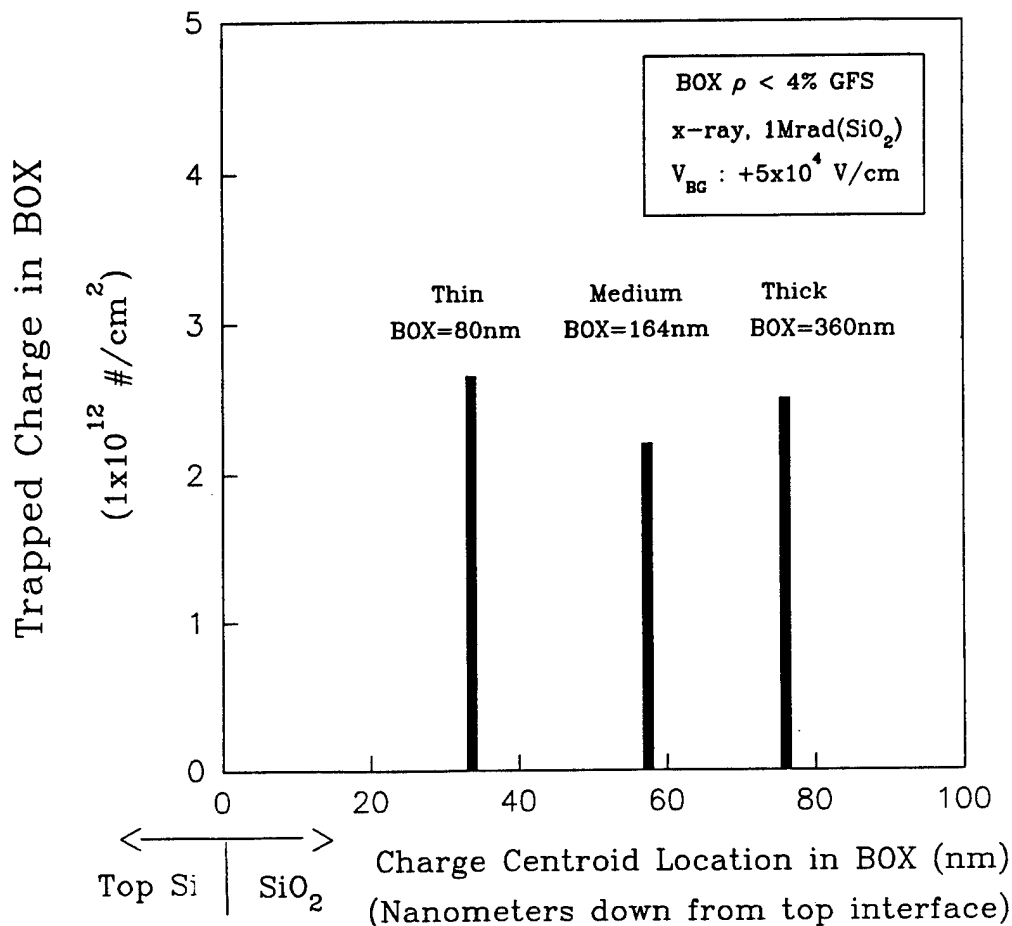
Figure 4-2. The centroid magnitude and location for three difference thicknesses. The radiation was done for V_{BG}:+5×10⁴ V/cm at 1Mrad (SiO₂).

in distance).

Now returning to Figure 4-1, what if a simple geometric correction is made to the centroid locations for the medium and thin BOX structures? Basically, if the thin BOX centroid is moved from 34nm to 76nm, where it is for the thickest sample, the interface should sense approximately half the trapped charge. Using this argument, the medium and thin BOX have been adjusted. The result is shown in Figure 4-3.

This geometric correction reestablishes the square-law dependence. Thus, the observed inflection point can be explained by the location of the charge centroid for the medium to thin non-saturated BOX structures.
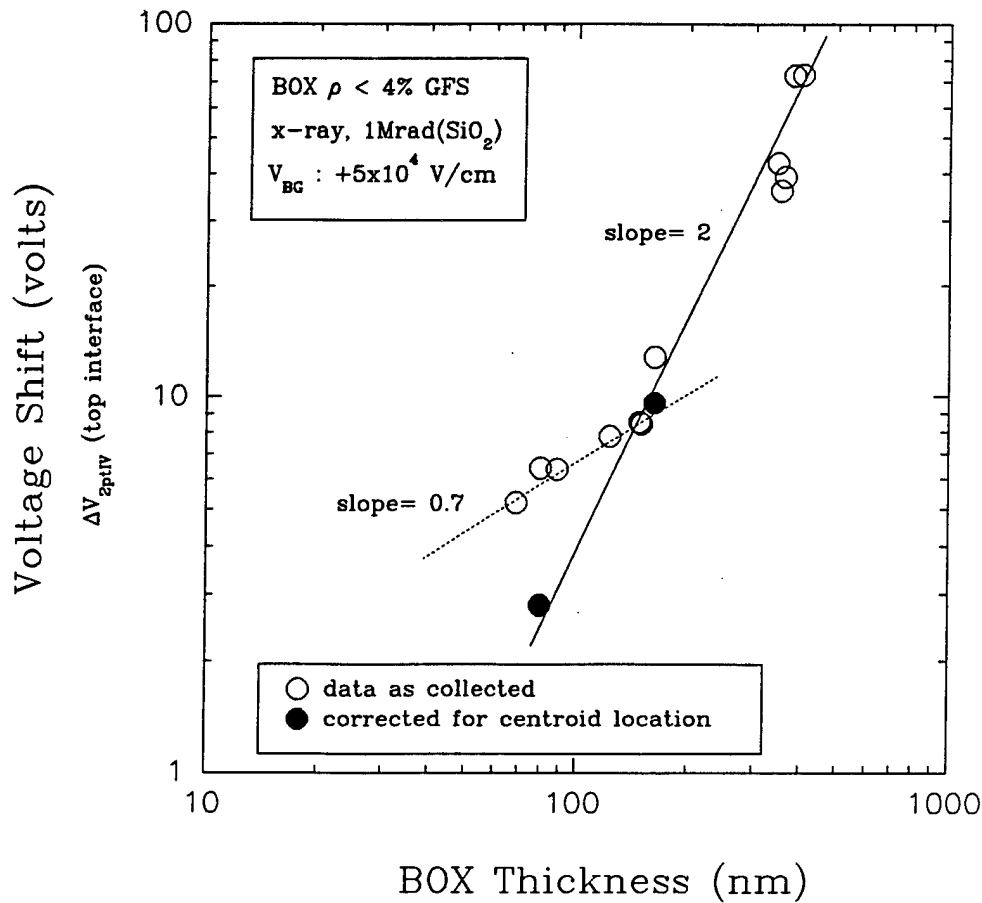
Figure 4-3. A re-plot of the V_{BG}:+5x10^4 V/cm data using a simple geometric correction for the medium and thin BOX centroid.

4.1.2 Motion of Radiation-Induced Holes.

To better understand the above observed BOX charge trapping phenomena, a more detailed knowledge of the total dose charge trapping response was needed. Figure 4-4 shows the total dose response for a BOX=350nm with low density and an applied fringing field of V_{BG}:+5x10^4 V/cm.

Note that the 1Mrad(SiO$_2$) location appears to be in the middle of the total dose curve. This location indicates a non-saturation condition within the BOX. The term non-saturation implies that the given process has not come to completion. The two processes involved here are; the radiation induced hole drift under the

20
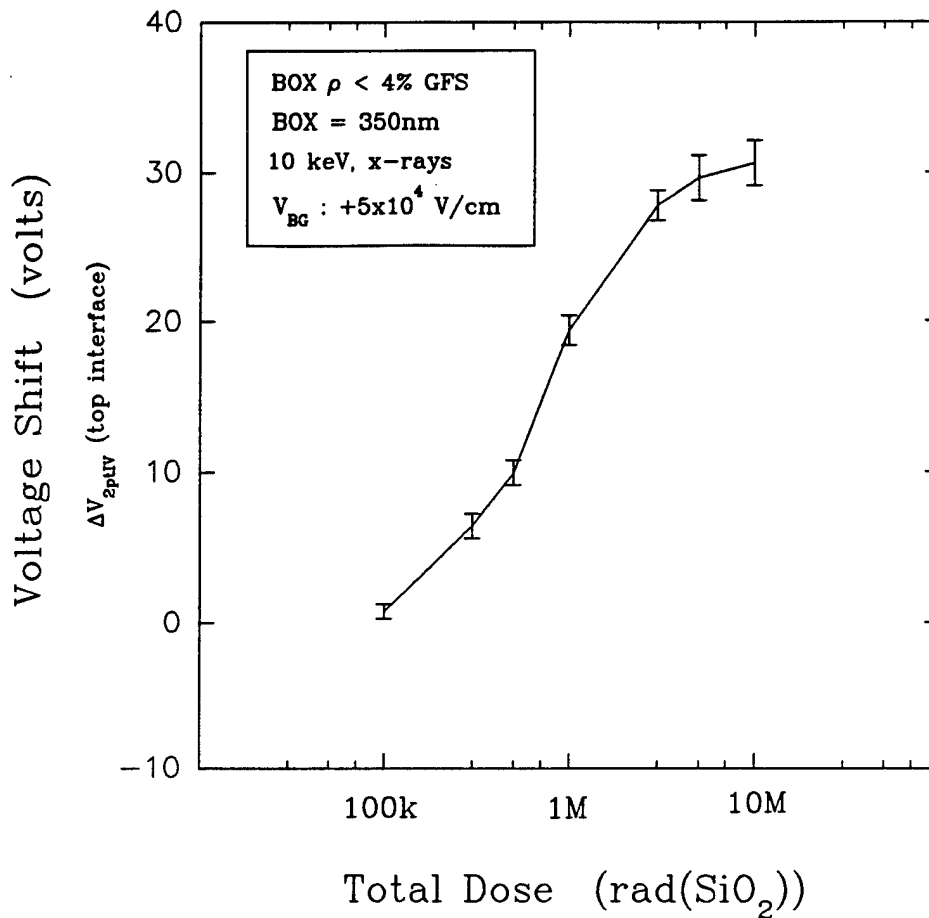
Figure 4-4. A total dose plot for V_{BG}:+5x10^4 V/cm. (The observed reduction in voltage shifts in Figure 4-4, as compared to Figure 4-1, is due to brief isothermal annealing at each dose location.)

influence of an applied electric field, and second, recombination. The more likely incomplete process here is the mobility of the holes.

Normally when comparing charge trapping among various oxides, only charge saturated conditions are considered. For this purpose a field of 5x10^5 V/cm was selected and a total dose evaluation was conducted. Figure 4-5 shows the total dose response for a 350nm BOX, low density, and with V_{BG}:+5x10^5 V/cm. Note that at a dose of 1Mrad(SiO$_2$) the BOX appears charge saturated.

21
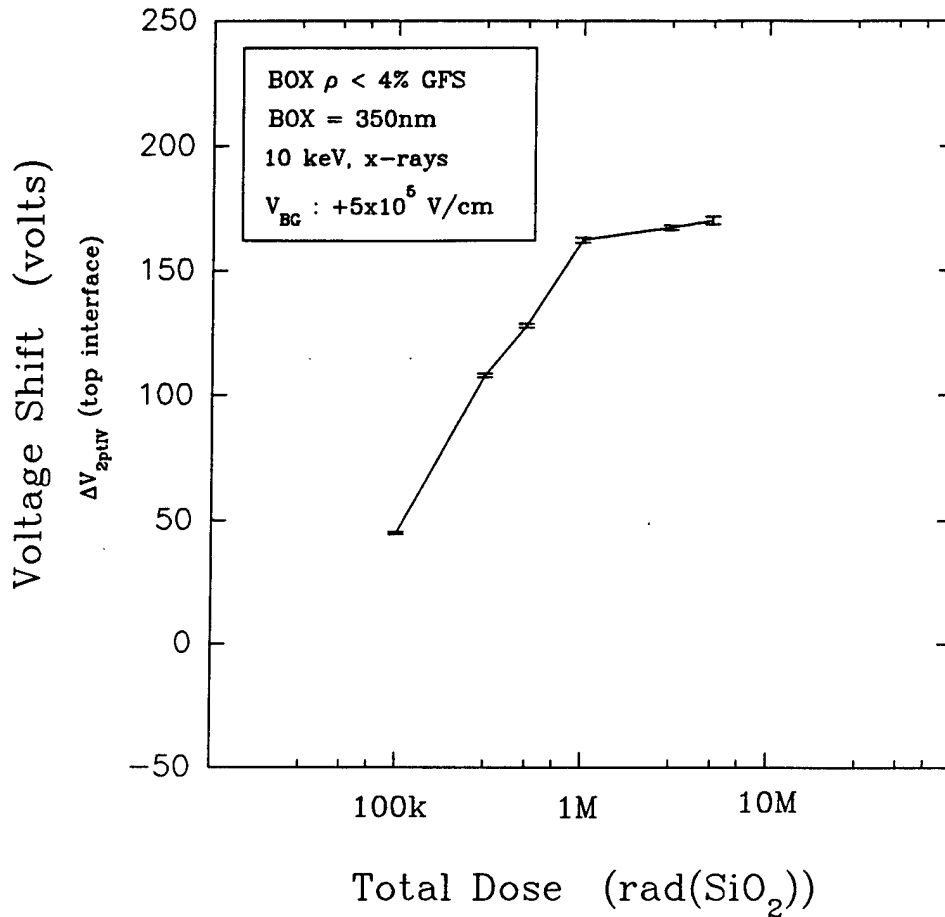
Figure 4-5. Voltage shift plot versus total dose for V_{BG}:+5×10^5 V/cm.

The voltage shift versus BOX thickness data for V_{BG}:+5×10^5 V/cm under a BOX-saturation condition is shown in Figure 4-6. The square-law dependence fits well. However the data in Figure 4-6 is related to an unrealistic device operating condition. The results from Figure 4-6 would be misleading to the applied "real-world" device designers. Namely, SOI components do not normally have such high fringing fields in the BOX region, and more importantly satellite systems are concerned with lower (non-saturation) level doses. The present emphasis is for components that can tolerate low field and low dose conditions. Charge trapping information from a saturation condition would be misleading to device designers.

22
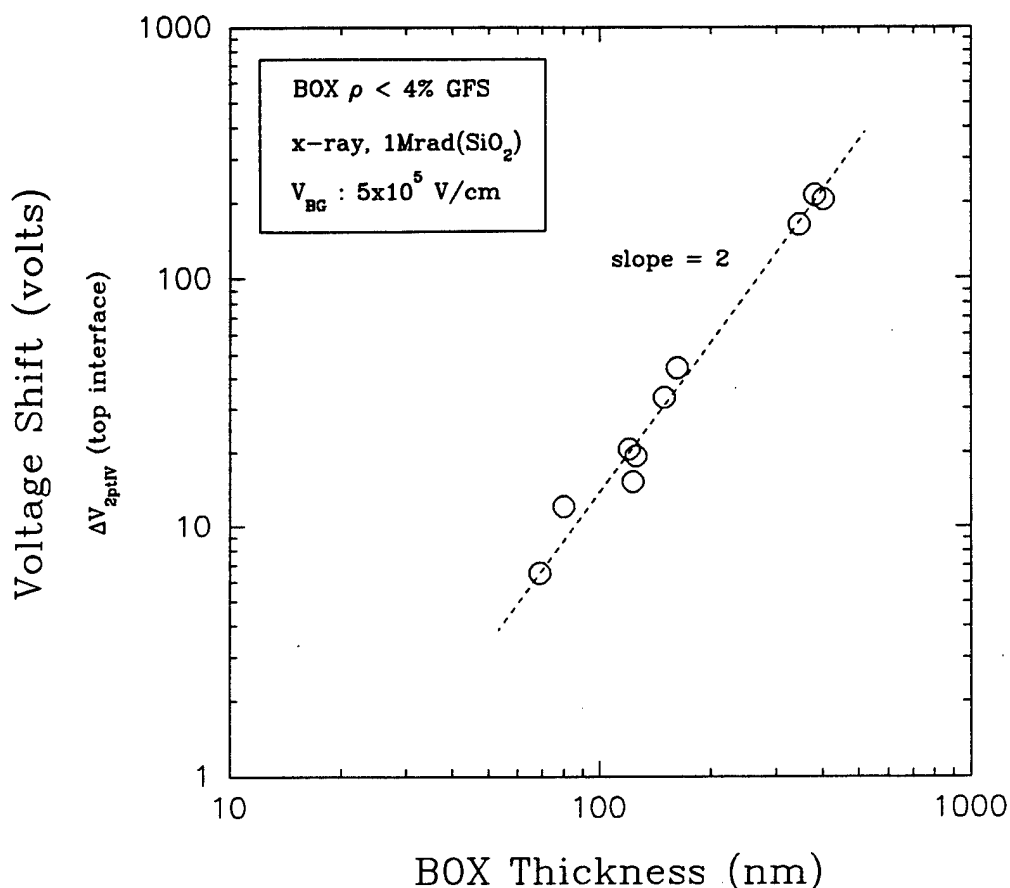
Figure 4-6. Voltage shift versus BOX thickness for V_{BG}:+5×10^5 V/cm at 1Mrad(SiO$_2$).

Even though the higher bias is a non-typical device electric field across the BOX, we investigated this saturation bias to gain insight into the BOX charge trapping mechanisms. Similar to above, selected dual C-V structures were repeated using V_{BG}:+5×10^5 V/cm 1Mrad(SiO$_2$). From these results an oxide charge centroid versus thickness relationship was obtained. Figure 4-7 shows the centroid location and magnitude for the three selected thicknesses. Note that in saturation the thicker the oxide the more charge is trapped in the BOX.

The charge to thickness relationship for this saturation condition is shown in Figure 4-8. Note the sub-linear
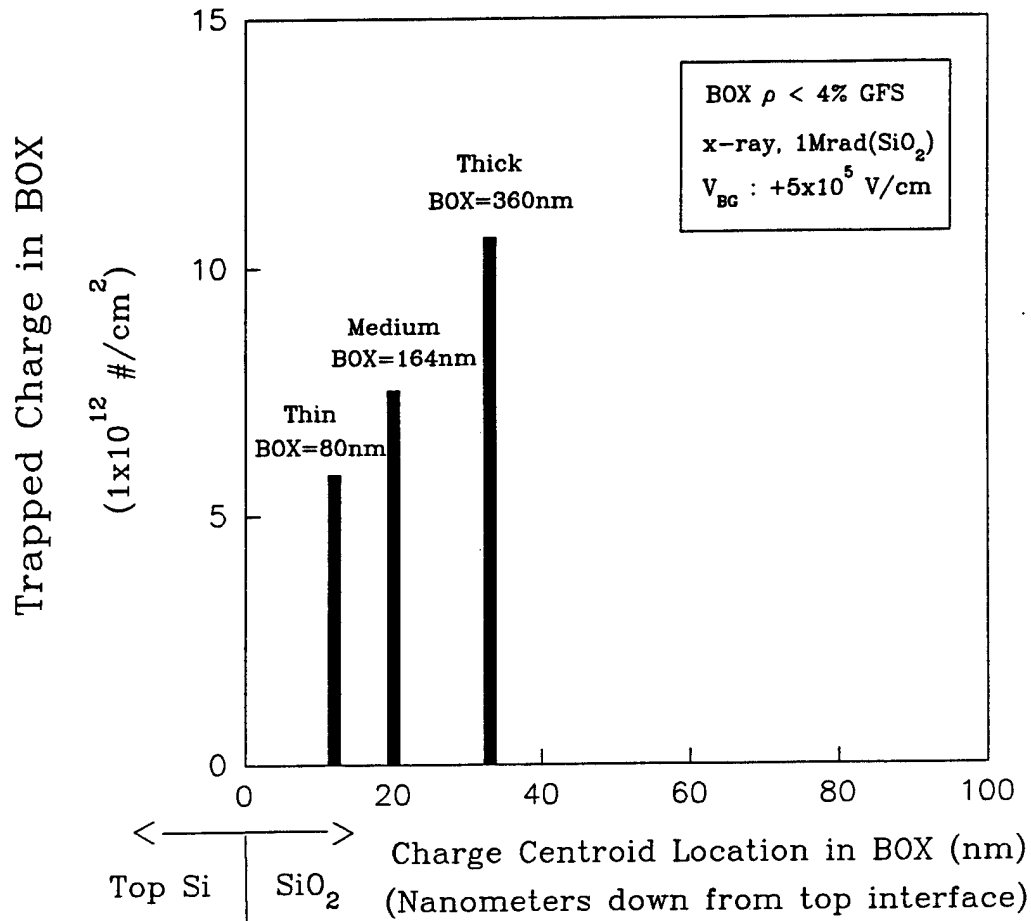
Figure 4-7. The centroid magnitude and location for three different thicknesses. The radiation was performed for V_{BG}:+5×10⁵ V/cm at 1Mrad(SiO₂).

relationship, which differs from that expected for a thermal oxide (a power of unity). It is known that SIMOX, due to the oxygen implantation process used to form the buried oxide, has bulk oxide trapping [21]; whereas, thermal oxides only have charge trapped at the Si-SiO₂ interface [1]. It would also be expected that the BOX charge centroid and magnitude might vary with thickness, due to the different levels of implant damage caused by the varying oxygen implant energies needed to form the various BOX thicknesses. An etch-back experiment would be necessary to obtain a detailed charge to thickness relationship needed to explain the above saturation square law behavior. At this point we present the above charge to thickness relationship

The chart shows a plot with y-axis labeled "Trapped Charge in BOX (1×10^{12} #/cm^2)" ranging from 1 to 100, and x-axis labeled "BOX Thickness (nm)" ranging from 10 to 1000. Legend box reads: "x-ray, 1Mrad(SiO$_2$)" and "V_{BG} : +5x10^5 V/cm".
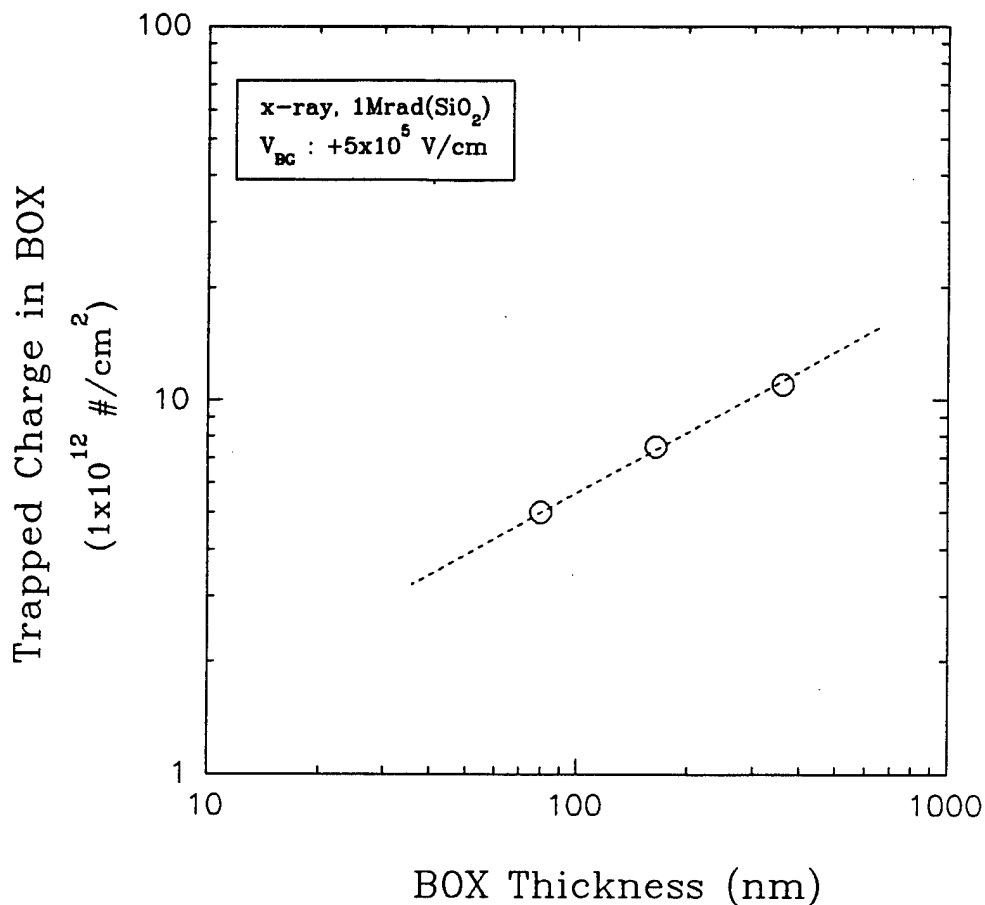
Figure 4-8. BOX trapped charge vs BOX thickness under saturation bias condition (V_{BG}:+5×10^5 V/cm, 1Mrad(SiO$_2$).

as an observational finding, and note that when the BOX is biased in saturation the square law dependence is observed.

To complete the bias range, other biases were also evaluated. Figure 4-9 shows voltage shift data versus BOX thickness for biases ranging from -5×10^5 V/cm to 5×10^5 V/cm. The negative biases show very little thickness dependence. From ground to 1×10^5 V/cm the inflection point is observed. Note the slope of the inflection point migrates into the square-law dependence as the applied bias during irradiation increases. This behavior is attributed to the centroid magnitude and location, which is now known to be influenced by the applied bias during irradiation and the BOX thickness.
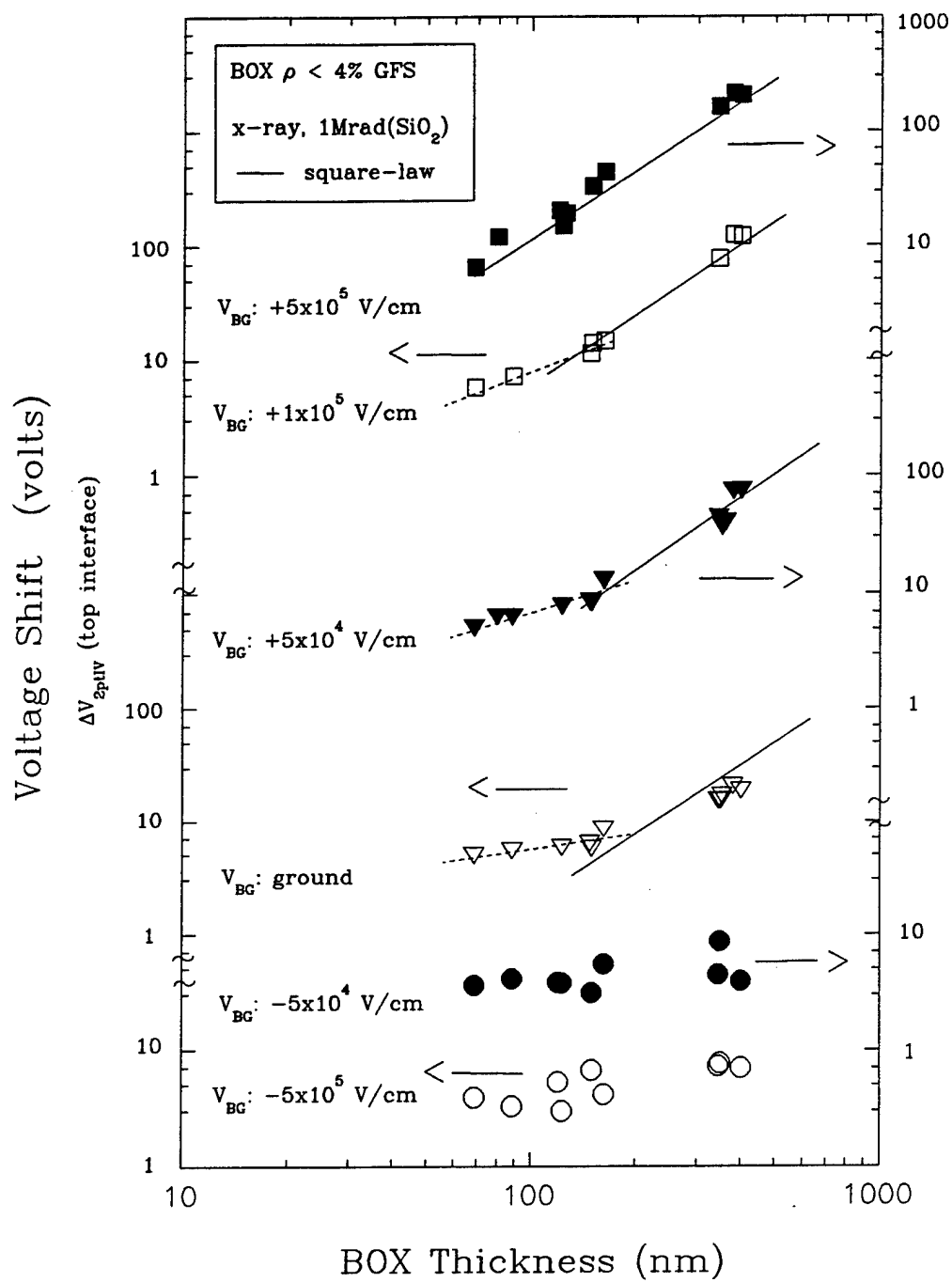
Figure 4-9. A group plot of voltage shift versus BOX thickness for various biases.

The main observation of this work is the appearance of an inflection point in the voltage shift versus BOX thickness relation for bias and radiation conditions typical of real applications. This inflection point is observed to appear at biases of ground and migrate into the square-law dependence at biases greater than V_{BG}:+5×10^5 V/cm. The inflection point can be removed by allowing the BOX to saturate in radiation induced charge buildup.

The results for the non-saturation condition can also be explained by considering the influence of the applied electric field during irradiation on the motion of the radiation induced holes versus the BOX thickness. The applied electric field (V_{BG}:positive) in this experiment causes the radiation induced holes to drift toward the top interface (simulating the pass-gate (source and drain "high") fringing field effect). For thin BOX material (<100nm) all the radiation induced holes are swept to the top interface. In the medium to thick BOX material only a fraction of the radiation induced holes drift to the top interface, due to hole mobility limitations. Increasing the applied field during irradiation increases the fraction of mobile holes that will make it to the top interface for the thicker material, thus removing the inflection point in the thickness relationship.

Thus, the observed inflection point is a phenomena of non-saturation, and results from the radiation induced holes in the BOX not being able to move the greater distances required by the thicker BOX structures. When the BOX is biased into saturation during irradiation, the holes drift as far as they can go under the influence of the applied electric field and avoid recombination.

The importance of this work is in the comparison of SIMOX material as technology moves from the standard thick BOX material (>340nm) to the thinner BOX material (<100nm, possibly fully depleted). Having an understanding of the charge trapping to thickness relationship will help in determining material improvements, and aid device designers to predict circuit response.

4.2 BURIED-OXIDE ELECTRON TRAPPING RESPONSE.

From the photo-injection current vs. voltage curves (not shown here), the total bulk electron trapped charge and an electron charge centroid can be determined [10,12,23]. In contrast to the C-V measurements, the photo I-V obtains information from both interfaces, and thus the total bulk trapped charge Q_T per area is

$$Q_T = (\epsilon_{BOX} / T_{BOX}) * (\Delta V_+ + \Delta V_-),$$

where ϵ_{BOX} is the permittivity of the oxide, T_{BOX} the BOX thickness, ΔV_+ is the voltage shift when injection occurs from the BOX/Si interface, and ΔV_- is the voltage shift when injection occurs from the Al/BOX interface. The total number of occupied traps N_T per area is

$$N_T = Q_T/q,$$

where q is the electron charge, and the position χ of the charge centroid from the Al/BOX interface is

$$\chi = T_{BOX} / (1 - \Delta V_- / \Delta V_+).$$

In addition, from the data in Figure 3-4, the electron capture cross sections can be determined [24]. The results of the above calculations are summarized in Table 4-1 for the materials provided by vendors A and B.

What can clearly be observed from Table I is that the HITOX process, when compared to the corresponding control, has a larger total number of occupied traps. This is in agreement with the increased electron trapping observed in Figure 3-4. No significant difference is observed in the centroid location. Also, no difference is observed in the electron trap capture cross sections between HITOX and control samples. Thus, the trap capture cross section can not account for the increase in electron trapping levels. Both the control and HITOX structures had the same three electron trap capture cross sections: 2×10^{-14} cm^2, 5×10^{-17} cm^2, and 1×10^{-17} cm^2 (approx. values). The two larger capture cross sections are associated with electron trapping at amorphous silicon clusters (the BOX is considered to be silicon rich), and the smallest cross section is associated with network defects within the BOX [25].

Table 4-1.   Listed are the total occupied charge (electron traps), the charge centroid, and the determined electron capture cross sections for the SIMOX standard and HITOX structures.

Vendor	Process	Trap Density		Centroid	Cross Section
		$1/cm^2$	% down		cm^2
A	C	$-3.1x10^{11}$	50%		$1x10^{-14}$, $7x10^{-17}$, $1x10^{-17}$
A	HITOX	$-9.4x10^{11}$	43%		$4x10^{-14}$, $5x10^{-17}$, $1x10^{-17}$
B	C	$-1.2x10^{12}$	39%		$3x10^{-14}$, $7x10^{-17}$, $2x10^{-17}$
B	HITOX	$-1.6x10^{12}$	42%		$3x10^{-14}$, $9x10^{-17}$, $3x10^{-17}$

SECTION 5
CONCLUSIONS

5.1 NOTEWORTHY RESULTS.

This work has compared the radiation induced charge trapping response versus buried oxide thickness on various SIMOX buried oxides. It has been observed that medium to thin BOX material (<180nm) deviates from the square-law dependence for conditions typical in actual applications. Increasing the applied field ($>=5\times10^5$ V/cm), or allowing the BOX to charge saturate during ionizing irradiation, returns the relationship to the square-law dependence. These observations are explained by the influence the applied electric field has during irradiation on the motion of radiation induced holes within the BOX. The observed inflection point was explained by the location and magnitude of the radiation induced BOX charge centroid and its relationship to BOX thickness.

In addition, this work has shown that the HITOX process causes an increase in the electron trapping for a SIMOX buried oxide. The increase can not be accounted for by changes in electron trap capture cross sections, nor by the influence of interface effects. Since these device electrical observables do not explain the HITOX's increase in net electron trapping, then the cause is likely an increase in trap generation resulting from the kinetics of the HITOX/BOX growth. Thus, the observed difference must be associated with the HITOX's process influence on the formation of HITOX/BOX oxide.

5.2 SUGGESTIONS FOR FUTURE INVESTIGATIONS.

The work in the above effort dealt with typical device application electric fields across the buried oxide (low fields). A possible suggestion for future experiments would be to investigate the saturation (high fields) total buried oxide trapped charge (top & bottom interface shifts) for various technologies (thin, thick, post-oxygen treated). The purpose would be to evaluate how the various technologies behave. Do thinner buried oxides (50nm - 200nm) trap more or less overall charge than thick (340nm - 400nm) buried oxides? The concern would be for a thin fully depleted technology where vertical charge control is important. For this thinner technology charge buildup at the lower (bottom, SiO_2/substrate) interface can be detrimental to the charge control of the device building top silicon film above. For the SIMOX technology to be of value in low power application, this charge control concern will be of importance.

SECTION 6
REFERENCES

1. T.P Ma, and P.V. Dressendorfer, *Ionizing Radiation Effects in MOS Devices & Circuits* (U), John Wiley & Sons, 152-153 (1989) (Unclassified).

2. R.K Lawrence, H.L. Hughes, and R.E. Stahlbush, "Radiation Sensitivity of Beam-Synthesized Oxides (U)," *Journal of Electronic Materials* Vol. 19, No. 7, 665-670 (1990) (Unclassified).

3. W.C. Jenkins and S.T. Liu, "Radiation Response Of Fully-Depleted MOS Transistors Fabricated in SIMOX (U)," *IEEE Trans. Nucl. Sci.* NS-41, No. 6, 2317-2321 (1994) (Unclassified).

4. S. Cristoloveanu, and S.S. Li, "*Electrical Characterization of Silicon-On-Insulator Materials and Devices*", Kluwer Academic Publishers, 1995 (Unclassified).

5. S. Nakashima, T. Katayama, Y. Miyamura, A. Matsuzaki, M. Imai, K. Izumi, and N. Ohwada, "Thickness Increment of Buried Oxide in a SIMOX Wafer by High-Temperature Oxidation (U)", *Proceeding 1994 IEEE International SOI Conference*, 71-72, Oct. 1994 (Unclassified).

6. Y. Takahashi, T. Ishiyama, and M. Tabe, "Counter-Oxidation of Superficial Si in Single-Crystalline Si on SiO_2 Structure (U)", *Appl. Phys. Lett.*, Vol. 65, No. 23, 2987-2989, Dec. 1994 (Unclassified).

7. T. Katayama, S. Nakashima, Y. Miyamura, M. Kataoka, M. Danbata, M. Imai, K. Izumi, and N. Ohwada, "Improvement of Surface Morphology of SIMOX Wafers by High-Temperature Oxidation (U)", *Proceeding 1994 IEEE International SOI Conference*, 75-76, Oct. 1994 (Unclassified).

8. A.J. Auberton-Herve', "New SOI-Based Applications (U)," *Proceeding 1993 IEEE International SOI Conference*, 8-9, Oct. 1993 (Unclassified).

9. Spectroscopic ellipsometry measurements (U) made by B.J. Mrstik of the Naval Research Laboratory and P.J. McMarr of SFA Inc. (Unclassified).

10. D.J. DiMaria, "Determination of Insulator Bulk Trapped Charge Densities and Centroids From Photocurrent-Voltage Characteristics of MOS Structures (U)", *J. Appl. Phys.*, Vol. 47, No. 9, 4073-4077, Sept. 1976 (Unclassified).

11. D.A. Buchanan and D.J. DiMaria, "Interface and Bulk Trap Generation in Metal-Oxide-Semiconductor Capacitors (U)", *J. Appl. Phys.*, Vol. 67, No. 12, 7439-7451, June 1990 (Unclassified).

12. E.H. Nicollian and J.R. Brews, *MOS (Metal Oxide Semiconductor) Physics and Technology*, John Wiley & Sons, 531-532, 1982 (Unclassified).

13. H.E. Boesch Jr., T.L. Taylor, and W.A. Krull, "Charge Trapping and Transport Properties of SIMOX Buried Oxide with a Supplemental Oxygen Implant (U)," *IEEE Trans. Nucl. Sci.* NS-40, No. 6, 1748-1754 (1993) (Unclassified).

14. S.T. Liu, P.S. Fechner, and R.L. Roisen, "Fast Turn Characterization of SIMOX Wafers (U)," IEEE SOS/SOI Technology Conference, 61-62 (1990) (Unclassified).

15. S.T. Liu, P.S. Fechner, and J. Schrankler, "Radiation Hardening of SIMOX Buried Oxides (U)," *Journal of Radiation Effects*, Vol. 12, No. 1, 40-44, (1991) (Unclassified).

16. S. Williams, S. Cristoloveanu, and G. Campisi, "Point Contact Pseudo-MOS Transistors in As-Grown Silicon on Insulator Wafers (U)," *Mat. Sci. and Engr.* B12, 191-194 (1992) (Unclassified).

17. J.H. Smith, R.K Lawrence, G.J. Campisi, "Numerical Analyses of Silicon-on-Insulator Short-Channel Effects in a Radiation Environment (U)," *Journal of Electronic Materials* Vol. 21, No. 7, 683-687 (1992) (Unclassified).

18. R.J. Krantz, L.W. Aukerman, and T.C. Zietlow, "Applied Field and Total Dose Dependence of Trapped Charge Buildup (U)," *IEEE Trans. on Nucl. Sci.*, NS-34, No. 6, 1196-1201, (1987) (Unclassified).

19. H.E. Boesch Jr., T.L. Thomas, L.R. Hite, and W.E. Bailey, "Time-Dependent Hole and Electron Trapping Effects in SIMOX Buried Oxides (U)," *IEEE Trans. on Nucl. Sci.*, NS-37, No. 6, 1982-1989, (1990) (Unclassified).

20. B.J. Mrstik, P.J. McMarr, R.K. Lawrence, and H.L. Hughes, "The Use of Spectroscopic Ellipsometry to Predict the Radiation Response of SIMOX (U)," *IEEE Trans. Nucl. Sci.* NS-41, No. 6, 2277-2283 (1994) (Unclassified).

21. C.A. Pennise and H.E. Boesch Jr., "Determination of The Charge-Trapping Characteristics of Buried Oxides Using a 10-KeV X-ray Source (U)," *IEEE Trans. Nucl. Sci.* NS-37, No. 6, 1990-1994 (1990) (Unclassified).

22. R.E Stahlbush, H.L. Hughes, and W.A. Krull, "Reduction of Charge Trapping in Electron Tunneling in SIMOX by Supplemental Implantation of Oxygen (U)," *IEEE Trans. Nucl. Sci.* NS-40, No. 6, 1740-1747 (1993) (Unclassified).

23. R.S. Muller and T.I. Kamins, *Device Electronics for Integrated Circuits*, John Wiley & Sons, 400-401 (1986) (Unclassified).

24. G. Barbottin, and A. Vapaille, "*Instabilities in Silicon Devices*," North-Holland, pp. 56-57, 1989 (Unclassified).

25. V.V. Afanas'ev, A.G. Revesz, G.A. Brown, and H.L. Hughes, "Deep and Shallow Electron Trapping in the Buried Oxide Layer of SIMOX Structures (U)," *J. Electrochem. Soc.*, Vol. 141, No. 10, pp. 2801-2806, Oct. 1994 (Unclassified).

DISTRIBUTION LIST
TR-96-12

DEPARTMENT OF DEFENSE

DEFENSE ELECTRONIC SUPPLY CENTER
    ATTN: DESC-E

DEFENSE INTELLIGENCE AGENCY
    ATTN: DT-1BT
    ATTN: TWJ

DEFENSE SPECIAL WEAPONS AGENCY
    ATTN: ESA, W SUMMA
    ATTN: ESE/L COHN
    ATTN: ESE/L PALKUTI
    ATTN: ESE, R C WEBB
 2CY ATTN: ISST

DEFENSE TECHNICAL INFORMATION CENTER
 2CY ATTN: DTIC/OCP

FC DEFENSE SPECIAL WEAPONS AGENCY
    ATTN: FCINI
    ATTN: FCTO
    ATTN: FCTT, DR BALADI

TECHNICAL RESOURCES CENTER
    ATTN: JNGO

DEPARTMENT OF THE ARMY

ADVANCED RESEARCH PROJECT AGENCY
    ATTN: ASST DIR (ELECTRONIC SCIENCES DIV)

ARMY RESEARCH LABORATORIES
    ATTN: AMSRL-PS-PD
    ATTN: AMSRL-WT-NJ
    ATTN: DR TIM OLDHAM

MDSTC
    ATTN: CSSD-WD

MISSILE DEFENSE & SPACE TECHNOLOGY CTR
    ATTN: CSSD-TC-SR

U S ARMY RESEARCH OFFICE
    ATTN: R GRIFFITH

USAISC
    ATTN: ASOP-DO-TL

DEPARTMENT OF THE NAVY

NAVAL RESEARCH LABORATORY
    ATTN: C DALE
    ATTN: D BROWN
    ATTN: A B CAMPBELL
    ATTN: N SAKS
    ATTN: H HUGHES

NAVAL WEAPONS SUPPORT CENTER
    ATTN: D PLATTETER

OFFICE OF NAVAL INTELLIGENCE
    ATTN: LIBRARY

PROGRAM EXECUTIVE OFFICE
    ATTN: AIR-536T

DEPARTMENT OF THE AIR FORCE

AIR FORCE CTR FOR STUDIES & ANALYSIS
    ATTN: AFSAA/SAI

AIR UNIVERSITY LIBRARY
    ATTN: AUL-LSE

PHILLIPS LABORATORY
    ATTN: CAPT CHARLES BROTHERS
    ATTN: PL/VTE
    ATTN: PL/VTEE, S SAMPSON
    ATTN: PL/WSC

ROME LABORATORY/CC
    ATTN: ESR

SMC/MCX
    ATTN: LT SCOTT BECHTLOFF

SMC/MTAX
    ATTN: K BASANY

USAF ROME LABORATORY TECHNICAL LIBRARY
    ATTN: RBR

WL/ELE BLDG 620
    ATTN: WL/ELE

WL/MTE
    ATTN: MTE

DEPARTMENT OF ENERGY

ALBUQUERQUE OPERATIONS OFFIC
    ATTN: NESD

LAWRENCE LIVERMORE NATIONAL LAB
    ATTN: L-84/G POMYKAL
    ATTN: W ORVIS

LOS ALAMOS NATIONAL LABORATORY
    ATTN: MS B230/E LEONARD

SANDIA NATIONAL LABORATORIES
    ATTN: F SEXTON
    ATTN: L D POSEY
    ATTN: P WINOKUR
    ATTN: T A DELLIN

OTHER GOVERNMENT

CENTRAL INTELLIGENCE AGENCY
    ATTN: OSWR/NED 5S09 NHB
    ATTN: OSWR/STD/MTB 5S09 NHB

GODDARD SPACE FLIGHT CENTER
    ATTN: V DANCHENKO
    ATTN: E STASSINOPOULOS
    ATTN: K LABEL

DEPARTMENT OF DEFENSE CONTRACTORS

ALLIED-SIGNAL, INC.
    ATTN: DOCUMENT CONTROL

ANALYTICAL SERVICES, INC. (ANSER)
    ATTN: A SHOSTAK

BOEING CO
    ATTN: M/S 2T-50 D EGELKROUT

BOOZ ALLEN & HAMILTON INC
    ATTN: D VINCENT
    ATTN: T J ZWOLINSKI

JET PROPULSION LAB
    ATTN: C BARNES

CHARLES STARK DRAPER LAB, INC.
    ATTN: J BOYLE

CLEMSON UNIVERSITY
    ATTN: P J MCNULTY

DATA SYSTEMS CORP
    ATTN: B RICKARD
    ATTN: K WRIGHT

DAVID SARNOFF RESEARCH CENTER, INC
    ATTN: R SMELTZER

DEFENSE GROUP, INC
    ATTN: ROBERT POLL

EATON CORP.
    ATTN: R BRYANT

GENERAL ELECTRIC CO (ASD)
    ATTN: D SWANT
    ATTN: D TASCA
    ATTN: H O'DONNELL
    ATTN: J ANDREWS
    ATTN: J LINNEN
    ATTN: J LOMAN

GENERAL ELECTRIC CO.
    ATTN: B FLAHERTY
    ATTN: L HAUGE

GEORGE WASHINGTON UNIVERSITY
    ATTN: A FRIEDMAN

HARRIS CORPORATION
    ATTN: E YOST
    ATTN: W ABARE

HONEYWELL INC
    ATTN: C SANDSTROM

HONEYWELL, INC.
    ATTN: MS 725-5

HUGHES AIRCRAFT COMPANY
    ATTN: E KUBO

IBM CORP.
    ATTN: A SADANA

JAYCOR
    ATTN: D WALTERS

TR-96-12 (DL CONTINUED)

JAYCOR
    ATTN: CYRUS P KNOWLES
    ATTN: R SULLIVAN

JOHN HOPKINS UNIVERSITY
    ATTN: R MAURER

KAMAN SCIENCES CORPORATION
    ATTN: DASIAC
    ATTN: R RUTHERFORD

LOCKHEED MARTIN CORPORATION
    ATTN: TECHNICAL INFORMATION CENTER

LOCKHEED MARTIN CORPORATION
    ATTN: G LUM
    ATTN: J CAYOT

LOCKHEED MARTIN FEDERAL SYSTEMS, INC
    ATTN: L ROCKETT
    ATTN: N HADDAD

LOGICON R AND D ASSOCIATES
    ATTN: D CARLSON

LORAL AERONUTRONIC
    ATTN: TECHNICAL LIBRARY

MARTIN MARIETTA
    ATTN: J MILLER

MARTIN MARIETTA DENVER AEROSPACE
    ATTN: RESEARCH LIBRARY

MARYLAND, UNIVERSITY OF
    ATTN: H C LIN

MAXWELL LABORATORIES INC
    ATTN: DR JASON WILKENFELD

MISSION RESEARCH CORP.
    ATTN: D ALEXANDER

MISSION RESEARCH CORP.
    ATTN: J LUBELL

MITRE CORPORATION
    ATTN: J R SPURRIER
    ATTN: M FITZGERALD

ORBITAL SCIENCE CORP.
    ATTN: ROB CHERNEY

PACIFIC-SIERRA RESEARCH CORP.
    ATTN: H BRODE

RAYTHEON CO.
    ATTN: D D LEE
    ATTN: JOSEPH SURRO

RESEARCH TRIANGLE INSTITUTE
    ATTN: M SIMONS

ROCKWELL CORP.
    ATTN: V DE MARTINO

SCIENCE APPLICATIONS INTL CORP
    ATTN: W CHADSEY

SCIENTIFIC RESEARCH ASSOC, INC.
    ATTN: H GRUBIN

SFA INC.
  2CY ATTN: A G REVESZ
  2CY ATTN: P J MCMARR
  2CY ATTN: R K LAWRENCE

SUNDSTRAND CORP.
    ATTN: C WHITE

SYSTRON-DONNER CORP
    ATTN: SECURITY OFFICER

TECHNOLOGY DEVELOPMENT ASSOCIATES
    ATTN: R V BENEDICT

TELEDYNE BROWN ENGINEERING
    ATTN: G R EZELL
    ATTN: LEWIS T SMITH
    ATTN: M P FRENCH

THE AEROSPACE CORP
    ATTN: D SCHMUNK
    ATTN: K G HOLDEN
    ATTN: LEE MENDOZA
    ATTN: N SRAMEK
    ATTN: R KOGA

THE RAND CORPORATION
    ATTN: C CRAIN

TR-96-12 (DL CONTINUED)

TRW
    ATTN: M J TAYLOR

TRW INC.
    ATTN: T.I.C., S/1930

TRW S. I. G.
    ATTN: C BLASNEK

TRW SPACE & DEFENSE SECTOR SPACE &
TECH GROUP OGDEN ENG OPERATIONS
    ATTN: D M LAYTON

UNISYS CORPORATION-DEFENSE SYSTEMS
    ATTN: P MARROFFINO

VISIDYNE INC.
    ATTN: C H HUMPHREY
    ATTN: W P REIDY